ARTICLE

Kv12-encoded K+ channels drive the day–night switch in the repetitive firing rates of SCN neurons

Tracey O. Hermanstyne[1] [iD], Nien-Du Yang[2,3] [iD], Daniel Granados-Fuentes[4] [iD], Xiaofan Li[5] [iD], Rebecca L. Mellor[2] [iD], Timothy Jegla[5] [iD], Erik D. Herzog[4] [iD], and Jeanne M. Nerbonne[1,2,3] [iD]

Considerable evidence suggests that day–night rhythms in the functional expression of subthreshold potassium (K+) channels regulate daily oscillations in the spontaneous firing rates of neurons in the suprachiasmatic nucleus (SCN), the master circadian pacemaker in mammals. The K+ conductance(s) driving these daily rhythms in the repetitive firing rates of SCN neurons, however, have not been identified. To test the hypothesis that subthreshold Kv12.1/Kv12.2-encoded K+ channels play a role, we obtained current-clamp recordings from SCN neurons in slices prepared from adult mice harboring targeted disruptions in the *Kcnh8* (Kv12.1$^{-/-}$) or *Kcnh3* (Kv12.2$^{-/-}$) locus. We found that mean nighttime repetitive firing rates were higher in Kv12.1$^{-/-}$ and Kv12.2$^{-/-}$ than in wild type (WT), SCN neurons. In marked contrast, mean daytime repetitive firing rates were similar in Kv12.1$^{-/-}$, Kv12.2$^{-/-}$, and WT SCN neurons, and the day–night difference in mean repetitive firing rates, a hallmark feature of WT SCN neurons, was eliminated in Kv12.1$^{-/-}$ and Kv12.2$^{-/-}$ SCN neurons. Similar results were obtained with in vivo shRNA-mediated acute knockdown of Kv12.1 or Kv12.2 in adult SCN neurons. Voltage-clamp experiments revealed that Kv12-encoded current densities in WT SCN neurons are higher at night than during the day. In addition, the pharmacological block of Kv12-encoded currents increased the mean repetitive firing rate of nighttime, but not daytime, in WT SCN neurons. Dynamic clamp-mediated subtraction of modeled Kv12-encoded currents also selectively increased the mean repetitive firing rates of nighttime WT SCN neurons. Despite the elimination of the nighttime decrease in the mean repetitive firing rates of SCN neurons, however, locomotor (wheel-running) activity remained rhythmic in Kv12.1$^{-/-}$, Kv12.2$^{-/-}$, and Kv12.1-targeted shRNA-expressing, and Kv12.2-targeted shRNA-expressing animals.

Introduction

Neurons in the suprachiasmatic nucleus (SCN), the master circadian pacemaker in mammals, including humans, display day–night oscillations in spontaneous repetitive firing rates that drive daily rhythms in physiology and behavior (Reppert and Weaver, 2001; Hastings et al., 2018, 2019; Michel and Meijer, 2020). In vivo recordings from the rat SCN, isolated from synaptic and humoral inputs, were the first to demonstrate cell-autonomous circadian rhythms in the electrical activity of the SCN, with neuronal firing rates higher during the day than at night (Inouye and Kawamura, 1979). Numerous subsequent studies have confirmed that the repetitive firing rates of SCN neurons are higher during the day than at night, with daytime firing rates averaging about 5 Hz and nighttime firing rates averaging about 1 Hz (Kuhlman and McMahon, 2006; Brown and Piggins, 2007; Allen et al., 2017; Belle and Allen, 2018;

Harvey et al., 2020). These daily rhythms in repetitive firing rates are accompanied by alterations in input resistances (higher during the day than at night) and membrane potentials (more depolarized during the day than at night), linked to daily changes in subthreshold potassium (K+) conductance(s) (Kuhlman and McMahon, 2006; Brown and Piggins, 2007; Allen et al., 2017; Belle and Allen, 2018; Harvey et al., 2020). An alternative "bicycle" model for the circadian regulation of membrane excitability in the SCN, involving a daytime increase in an inward Na+ leak current (causing membrane depolarization and increased firing) and a nighttime increase in a K+ current (causing membrane hyperpolarization and decreased firing), has also been proposed (Flourakis et al., 2015). The daytime depolarization in the membrane potentials of SCN neurons, however, is associated with increased, not decreased,

....
[1]Department of Developmental Biology, Washington University School of Medicine, St. Louis, MO, USA;   [2]Cardiovascular Division, Department of Medicine, Washington University School of Medicine, St. Louis, MO, USA;   [3]Department of Biomedical Engineering, Washington University, St. Louis, MO, USA;   [4]Department of Biology, Washington University, St. Louis, MO, USA;   [5]Department of Biology, The Pennsylvania State University, University Park, State College, PA, USA.

Correspondence to Jeanne M. Nerbonne: jnerbonne@wustl.edu

input resistance, as would result from opening inward Na^{+} leak channels. Even in the bicycle model (Flourakis et al., 2015), therefore, a reduction in daytime K^{+} conductance is required. Interestingly, this daily pattern (higher firing rates and input resistances during the day than at night) is observed in both diurnal and nocturnal animals (Nunez et al., 1999; Kumar Jha et al., 2015), suggesting that the underlying molecular mechanism(s) is conserved.

Although the daily oscillations in the membrane potentials and input resistances of SCN neurons indicate that day–night changes in subthreshold K^{+} conductance(s) are required for rhythmic changes in repetitive firing rates, the critical K^{+} conductance(s) has not been identified (Brown and Piggins, 2007; Allen et al., 2017; Belle and Allen, 2018; Harvey et al., 2020). Several studies have identified roles for voltage-gated K^{+} (Kv) channels encoded by the *Kcnc1* (Kv3.1; Itri et al., 2005; Kudo et al., 2011), *Kcnc2* (Kv3.2; Itri et al., 2005; Kudo et al., 2011), *Kcna4* (Kv1.4; Granados-Fuentes et al., 2012, 2015), *Kcnd1* (Kv4.1; Itri et al., 2010; Hermanstyne et al., 2017), and *Kcnd2* (Kv4.2; Itri et al., 2010; Granados-Fuentes et al., 2012, 2015) pore-forming (α) subunits and for large conductance voltage- and Ca^{2+}-dependent K^{+} (BK) channels (Meredith et al., 2006; Kent and Meredith, 2008; Whitt et al., 2016) in regulating the repetitive firing rates of SCN neurons. Although day–night differences in the densities of several of these K^{+} currents (Itri et al., 2005, 2010; Meredith et al., 2006; Kudo et al., 2011; Hermanstyne et al., 2017) and in the expression levels of transcripts (http://circadb.hogeneschlab.org) encoded by the underlying K^{+} channel subunit genes (Itri et al., 2005; Meredith et al., 2006) have been reported, none of these K^{+} channels has been shown to control the day–night switch in the input resistances, membrane potentials, and spontaneous repetitive firing rates of SCN neurons (Brown and Piggins, 2007; Allen et al., 2017; Belle and Allen, 2018; Harvey et al., 2020). The K^{+} conductance(s) driving the cell-autonomous circadian rhythms in the repetitive firing properties of SCN neurons remain to be identified. Similar to other types of central and peripheral neurons, in situ hybridization and quantitative RNA expression profiling data show that transcripts encoding a number of other K^{+} channel α subunits are expressed in the SCN (Panda et al., 2002; Harvey et al., 2020). Of particular note are two members of the *Ether-à-go-go-like* (*Elk*) subfamily of Kv channel α subunits, *Kcnh8* and *Kcnh3*, which encode the Kv12.1 and Kv12.2 α subunits, respectively, and are predominantly expressed in the brain (Engeland et al., 1998; Miyake et al., 1999; Zou et al., 2003). Heterologous expression studies have demonstrated that Kv12.1 or Kv12.2 generate voltage-gated outward K^{+} currents that activate at subthreshold membrane potentials (Trudeau et al., 1999; Becchetti et al., 2002; Zou et al., 2003; Zhang et al., 2009, 2010; Li et al., 2015), but display marked differences in inactivation: Kv12.2-encoded currents partially inactivate at depolarized membrane potentials (greater than +20 mV), whereas Kv12.1-encoded outward currents do not (Engeland et al., 1998; Miyake et al., 1999). The voltage-dependences of activation of Kv12.x-encoded K^{+} currents are affected by Zn^{2+} and some (but not all) other divalent cations (Zhang et al., 2010) and are modulated by phosphatidylinositol 4,5-bisphosphate (Li et al., 2015) and

extracellular pH (Zhang et al., 2009). In addition, it has been demonstrated that heterologously expressed Kv12.1 and Kv12.2 (and 12.3) α subunits coassemble (Trudeau et al., 1999; Becchetti et al., 2002; Zou et al., 2003; Zhang et al., 2010; Li et al., 2015), although it remains to be determined if heteromeric Kv12.x channels are present in native cells. Interestingly, however, it has been reported that the targeted disruption of the *Kcnh3* (Kv12.2) locus increased the input resistances and depolarized the resting membrane potentials of CA1 hippocampal pyramidal neurons (Kazmierczak et al., 2013). In addition, smaller currents were required to evoke action potentials, and the evoked repetitive firing rates were higher in Kv12.2[−/−] compared with wild-type (WT), CA1 hippocampal neurons (Kazmierczak et al., 2013). The experiments here were designed to test directly the hypothesis that Kv12.1- and/or Kv12.2-encoded K^{+} channels underlie the subthreshold K^{+} conductance that reduces the excitability of mouse SCN neurons at night. Combining in vivo molecular genetic strategies to manipulate Kv12.1 or Kv12.2 expression with in vitro electrophysiological and pharmacological approaches to assess the functional consequences of these manipulations, the experiments detailed here demonstrate a critical role for Kv12-encoded K^{+} channels in regulating the nighttime repetitive firing rates and in controlling the day–night rhythms in the repetitive firing rates of SCN neurons.

Materials and Methods
All reagents were obtained from Sigma-Aldrich unless otherwise noted.

Animals
All procedures involving animals were approved by the Animal Care and Use Committee of Washington University and were conducted in accordance with the United States National Institutes of Health Guidelines for the Care and Use of Laboratory Animals. WT mice were C57BL/6J. The generation of the Kv12.2[−/−] mouse line, harboring a targeted disruption in the *Kcnh3* locus, also maintained in the C57BL/6J background, has been described previously. (Zhang et al., 2010). A similar strategy (illustrated in Fig. S1) was used to generate the Kv12.1[−/−] line lacking *Kcnh8*. Crossing Kv12.1[−/−] and Kv12.2[−/−] mice provided the Kv12.1[−/−]/Kv12.2[−/−] double knockout (DKO) line. All mice were maintained in the C57BL/6J background in one of the Washington University Danforth or Medical School animal facilities.

Screening of Kv12.1- and Kv12.2-targeted shRNAs
An interfering RNA strategy (Du et al., 2006) was developed to allow the acute in vivo knockdown of Kv12.1 or Kv12.2 expression selectively in the SCN of adult animals. In initial screening experiments, short hairpin RNA (shRNA) sequences targeting Kv12.1 (*n* = 5) or Kv12.2 (*n* = 5), obtained from the RNAi Consortium (TRC) through the Genome Institute at Washington University Medical School, were evaluated in vitro to determine the efficiency of Kv12.1 or Kv12.2 knockdown. For screening, tsA201 cells were cotransfected, using PepMute (Signagen), with a cDNA construct encoding Kv12.1-eYFP or Kv12.2-eYFP and one

of the Kv12.1-targeted or Kv12.2-targeted shRNAs. Additional experiments were conducted using a non-targeted (NT), control shRNA generated against a variant of green fluorescent protein. Approximately 48 h following the transfections, cell lysates were prepared, fractionated by SDS-PAGE, transferred to poly-vinylidene fluoride (PVDF) membranes, and probed for eYFP expression (#AB3080; polyclonal anti-GFP antibody, 1:1,000; Sigma Aldrich). Following imaging, these blots were probed with an α-tubulin antibody (#AB7291; monoclonal anti-α-tubulin, 1:10,000; Abcam) to verify equal protein loading of each lane and imaged again. The efficiency of the knockdown of Kv12.1-eYFP or Kv12.2-eYFP by each of the Kv12.1- or Kv12.2-targeted shRNAs was quantified by densitometry. The Kv12.1- and Kv12.2-targeted shRNA sequences producing the largest (~80%) reduction in Kv12.1-eYFP (5′-CAACATTAACTCAGGAGGTTT-3′) or Kv12.2-eYFP (5′-CAGCTTTATGGACCTCCACTT-3′) expression were subsequently evaluated for specificity. In these experiments, tsA201 cells were cotransfected with cDNA constructs encoding Kv12.1-eYFP, Kv12.2-eYFP, or Kv4.1-eYFP, together with the Kv12.1-targeted shRNA, Kv12.2-targeted shRNA, or NT shRNA. 2 d after the transfections, lysates were prepared and fractionated as described above. Western blots were probed first with the polyclonal anti-GFP antibody and imaged, followed by probing with the monoclonal anti-α-tubulin antibody and imaged again.

Generation of shRNA-expressing adeno-associated viruses
The selected Kv12.1-targeted, Kv12.2-targeted, and NT shRNA 21-nucleotide sense sequences were synthesized (Integrated DNA Technologies) into the corresponding 97-nucleotide microRNA-adapted shRNA oligonucleotides containing sense and antisense sequences linked by a 19-nucleotide hairpin loop. Forward and reverse strands were annealed and cloned in a microRNA (human miR30) context into the 3′-untranslated region (3′-UTR) of eGFP in the pPRIME vector (Stegmeier et al., 2005). The entire eGFP-shRNA cassette was then cloned into a viral shuttle vector with a synapsin (SYN) promoter. Adeno-associated viruses, serotype 8 (AAV8), shown previously to produce robust transduction of adult mouse SCN neurons in vivo (Hermanstyne et al., 2017) were generated by the Hope Center Virus Core Facility at Washington University Medical School.

Stereotaxic virus injections
Bilateral stereotaxic injections of the NT, the Kv12.1-targeted, or the Kv12.2-targeted shRNA-expressing AAV8 were made into the SCN of adult (6–10 wk) WT C57BL/6JN male and female mice using previously described methods (Hermanstyne et al., 2017). Briefly, under sterile conditions, each mouse was anesthetized with isoflurane (3%) and secured in a stereotaxic head frame (Kopf Instruments). The head was shaved and Betadine was applied to cleanse and sterilize the shaved region. An incision was then made along the midline and the skin was pulled back to expose the skull. One of the shRNA-expressing viruses was injected (~600 nl) into each hemisphere of the SCN (coordinates: 0.3 mm rostral to bregma, 0.1 mm left and right to the midline, and 5.6 mm ventral to the pial surface). The injection syringe

(Hamilton) delivered the virus at a constant rate of 0.1 μl/min using a syringe pump (KD Scientific). The syringe was left in place for ~5 min after the injection was completed to minimize the upward reflux of solution during the removal of the needle. Vetabond tissue adhesive (3M) was used to close the incision. Immediately following the surgery, animals were allowed to recover from the anesthesia on a heating pad maintained at 37°C and were given an intraperitoneal (IP) injection of Rimadyl (0.1 ml of 0.05 mg/ml; Pfizer).

Preparation of SCN slices
SCN slices (300 μm) were prepared from adult (8–12 wk old) WT, Kv12.1$^{-/-}$, Kv12.2$^{-/-}$, and Kv12.1$^{-/-}$/Kv12.2$^{-/-}$ (DKO) mice, maintained in either a standard (lights on at 7:00 am and lights off at 7:00 pm) or a reversed (lights on at 7:00 pm and lights off at 7:00 am) 12:12 h light–dark (LD) cycle, using previously described methods (Granados-Fuentes et al., 2012, 2015; Hermanstyne et al., 2017). Zeitgeber times (ZT) are indicated: ZT0 corresponds to the time of lights on and ZT12 to the time of lights off in the animal facility. Daytime slices were routinely prepared at ZT5 from WT, Kv12.1$^{-/-}$, Kv12.2$^{-/-}$, and DKO mice maintained in the standard LD cycle, and nighttime slices were routinely prepared at ZT16 from WT, Kv12.1$^{-/-}$, Kv12.2$^{-/-}$, and DKO mice maintained in the reversed LD cycle. Using a similar strategy, SCN slices were also prepared from mice 2 wk following NT, Kv12.1-targeted, or Kv12.2-targeted shRNA-expressing AAV8 injections into the SCN. In an additional set of experiments designed to determine if firing rates were affected at any time during the cycle, slices were also obtained from Kv12.1$^{-/-}$ and Kv12.2$^{-/-}$ animals during the transition from "lights-on to lights-off" (ZT12–ZT14), as well as slices prepared mid-day (ZT6–ZT8) and mid-evening (ZT18–ZT20).

For the preparation of daytime slices, brains were rapidly removed (in the light) from animals anesthetized with 1.25% Avertin (Acros Organics, 2,2,2-tribromoethanol and tert-amyl alcohol in 0.9% NaCl; 0.025 ml/g body weight) and placed in ice-cold cutting solution containing (in mM) 240 sucrose, 2.5 KCl, 1.25 NaH$_2$PO$_4$, 25 NaHCO$_3$, 0.5 CaCl$_2$, and 7 MgCl$_2$, saturated with 95% O$_2$/5% CO$_2$. In separate experiments, some daytime slices were prepared at ZT3 and ZT11 to obtain electrophysiological recordings earlier in the day (ZT6–ZT8) and during the transition from lights on to lights off (ZT12–ZT14). For the preparation of nighttime slices, animals in the reversed LD cycle were removed from their cages at ZT15 under infrared illumination, anesthetized with isoflurane, and enucleated using previously described procedure. (Aton et al., 2004; Hattar et al., 2006; Hermanstyne et al., 2016). Following an IP injection of Rimadyl (0.1 ml of 0.05 mg/ml), each animal was allowed to recover from the anesthesia (for ~1 h) prior to the preparation of slices. At ZT16, animals were anesthetized with 1.25% Avertin; brains were rapidly removed and placed in ice-cold cutting solution. For all experiments, coronal slices (300 μm) were cut on a Leica VT1000 S vibrating blade microtome (Leica Microsystems Inc.) and incubated in a holding chamber with oxygenated artificial cerebrospinal fluid (ACSF) containing (in mM) 125 NaCl, 2.5 KCl, 1.25 NaH$_2$PO$_4$, 25 NaHCO$_3$, 2 CaCl$_2$, 1 MgCl$_2$,

Hermanstyne et al.
Kv12 channels regulate nighttime SCN neuronal firing

Journal of General Physiology
https://doi.org/10.1085/jgp.202213310

3 of 23

and 25 dextrose ($\sim$310 mOsmol l^{-1}), saturated with 95% O$_2$/5% CO$_2$, at room temperature (23–25°C) for at least 1 h before transfer to the recording chamber.

Electrophysiological recordings

Whole-cell current-clamp and action potential- (voltage-) clamp recordings were obtained at room temperature (23–25°C) during the day (ZT7–ZT12) or at night (ZT18–ZT24) from SCN neurons in slices prepared (as described above) during the day or at night from WT, Kv12.1$^{-/-}$, Kv12.2$^{-/-}$, or DKO (Kv12.1$^{-/-}$/Kv12.2$^{-/-}$) mice. Current-clamp recordings were also obtained from SCN neurons in slices prepared during the day or at night 2 wk following NT, Kv12.1-targeted, or Kv12.2-targeted shRNA-expressing AAV8 injections. In all cases, several animals of each genotype (N = 3–9), with one slice from each animal (N) was used, and electrophysiological data were collected from multiple SCN neurons (n) in each slice. For recordings, SCN neurons were visually identified in slices using differential interference contrast optics with infrared illumination. Slices were perfused continuously with ACSF containing 20 µM Gabazine (Tocris Bioscience) and saturated with 95% O$_2$/5% CO$_2$. Whole-cell current-clamp recordings were obtained using pipettes (4–7 MΩ) containing (in mM) 144 K-gluconate, 10 HEPES, 3 MgCl$_2$, 4 MgATP, 0.2 EGTA, and 0.5 NaGTP (pH 7.3; 300 mOsmol l^{-1}). Using this (K-gluconate) pipette solution, the liquid junction potential was –16.4 mV; junction potentials were not corrected.

For each cell, a loose patch, cell-attached recording was first obtained, and the spontaneous repetitive firing of action potentials was recorded for $\sim$1 min. This was done routinely prior to establishing the whole-cell recording configuration. Following the formation of a gigaOhm seal, the whole-cell configuration was established, and whole-cell membrane capacitances and series resistances were compensated. Whole-cell spontaneous firing activity was then recorded again for $\sim$1 min and compared with the data acquired in the cell-attached mode. If any differences in the frequency and/or pattern of repetitive firing in the cell-attached and whole-cell recording configurations were evident, recordings were terminated, and any data acquired from these cells were not included in the analyses. Access resistances were 15–20 MΩ, and data acquisition was terminated if the access resistance increased by ≥20%. Voltage signals were acquired at 100 kHz, filtered at 10 kHz, and stored for offline analysis. Data were collected using a Multiclamp 700B patch clamp amplifier (Molecular Devices) interfaced to a Dell personal computer with a Digidata 1332 and the pCLAMP 10 software package (Molecular Devices). Consistent with previous studies (Itri et al., 2005; Meredith et al., 2006; Kudo et al., 2011; Granados-Fuentes et al., 2015; Hermanstyne et al., 2016; Mazuski et al., 2018), these loose-patch (extracellular) and whole-cell (intracellular) recordings revealed that daytime and nighttime adult mouse SCN neurons display tonic and irregular spontaneous repetitive firing patterns. To facilitate a comparison of repetitive firing rates across groups, the average repetitive firing rate of each cell during the initial 1 min of recording was determined. Mean ± SEM repetitive firing

rates for each group were calculated and are reported here. Input resistances (R$_{in}$) were determined by measuring the steady-state voltage changes produced by ±5 pA current injections from a membrane potential of –70 mV. The voltage threshold for action potential generation in each cell was determined as the point during the upstroke (depolarizing phase) of the action potential at which the second derivative of the voltage was zero. Resting membrane potentials (V$_r$) were estimated from phase plots of spontaneous action potentials. For each cell, the first derivative of the membrane potential (dV/dT) was plotted versus the membrane potential (mV), and V$_r$ was defined as the point where dV/dT = 0 during the interspike interval.

For action potential- (voltage-) clamp recordings, 0.1 mM CdCl$_2$ and 1 µM tetrodotoxin (TTX) were added to the standard ACSF bath solution described above. Recording pipettes (3–5 MΩ) contained (in mM) 144 K-gluconate, 10 HEPES, 3 MgCl$_2$, 4 MgATP, 0.2 EGTA, and 0.5 NaGTP (pH 7.3; 300 mOsmol l^{-1}). Spontaneous repetitive firing activity, recorded from a nighttime WT SCN neuron, was used as the voltage command. Tip potentials were zeroed before membrane-pipette seals were formed. Following the formation of a gigaOhm seal and establishing the whole-cell configuration, membrane capacitances and series resistances were compensated electronically. Series resistances were in the range of 15–20 MΩ and were routinely compensated by 70–80%. If the series resistance changed ≥20% during a recording, the experiment was stopped and the acquired data from that cell were not included in the analyses. Outward K$^+$ currents evoked in WT and DKO nighttime and daytime SCN neurons by the action potential voltage command were recorded in TTX- and CdCl$_2$-containing ACSF bath solution before and after application of 20 µM CX4 dissolved in the same (TTX- and CdCl$_2$-containing) ACSF bath solution. The CX4 (1-(2-chloro-6-methylphenyl)-3-(1,2-diphenylethyl) thiourea), developed by Dr. Timothy Jegla and colleagues at the Novartis Research Foundation (La Jolla, CA) and described as a selective blocker of heterologously expressed Kv12.2-encoded K$^+$ currents (Zhang et al., 2010), was provided by Dr. Jegla. Off-line digital subtraction of the outward K$^+$ currents recorded after local application of CX4 from the currents recorded prior to CX4 application provided the CX4-sensitive K$^+$ currents.

Additional experiments were conducted to determine the voltage dependence of activation of the CX4-sensitive currents in nighttime WT SCN neurons. To determine the voltage-dependence of activation of the CX4-sensitive currents, whole-cell Kv currents, evoked in response to 2 s depolarizing voltage steps to potentials between –100 and +50 mV (in 10 mV increments) from a holding potential (HP) of –70 mV, were first recorded in standard ACSF solution containing tetraethylammonium (10 mM), 4-aminopyridine (10 mM), CdCl$_2$ (0.1 mM), and tetrodotoxin (1 µM). Outward Kv currents, evoked using the same protocol, were recorded again (from the same cell) with CX4 (20 µM) added to the same ACSF solution. Off-line digital subtraction of the Kv currents recorded with and without the CX4 in the bath provided the CX4-sensitive currents (I$_{CX4}$; Fig. S2 A). In each cell, I$_{CX4}$ conductances at each test potential were calculated

and normalized to the maximal conductance (G_{max}) determined in the same cell. Mean ± SEM normalized I_{CX4} conductances (G/G_{max}) were then plotted as a function of the test potential and fitted using the Boltzmann equation, $G/G_{max} = 1 + e^{[(V_a - V_m)/k]}$ (Fig. S2 B), where V_a is the voltage of half-maximal activation and k is the slope factor.

Modeling Kv12-encoded (I_{Kv12}) and A-type (I_A) currents and dynamic clamp recordings

A three-state Markov model of I_{Kv12} channel gating, with two closed states, C_1 and C_2, and one open state, O, was developed using MATLAB (MathWorks Inc) using published kinetic and steady-state activation and deactivation data for heterologously expressed Kv12.1-encoded channels (Engeland et al., 1998; Scheme 1).
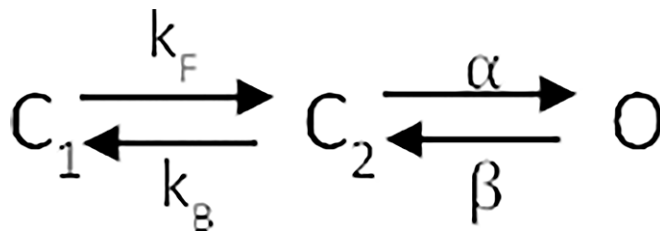
Scheme 1

The voltage-dependent forward and reverse transition rates, α and β, between the C_2 and O states, determined from the published data (Engeland et al., 1998), were $p_1\exp(p_2V_m)$ and $p_3\exp(-p_4V_m)$, respectively, where V_m is the membrane voltage, $p_1 = 0.019$, $p_2 = 0.065$, $p_3 = 0.011$, and $p_4 = -0.039$ (Clerx et al., 2019). The voltage-independent transition rates (k_F and k_B) between the C_1 and C_2 states were approximated from the published time constants of slow activation and the ratio of the fast and slow components of activation of Kv12.1-encoded currents (Engeland et al., 1998). The values determined for k_F and k_B were 0.008 and 0.0013, respectively. The steady-state voltage-dependence of activation of the model was then adjusted using the voltage-clamp data acquired from SCN neurons with a Kv12-selective inhibitor CX4 (see: Fig. S2, A and B). The Kv12 current is calculated as $I_{Kv12} = G*P(O)*(V_m - E_K)$, where G is a scalable parameter for current magnitude, P(O) is the probability that the channel is open, and E_K is the reversal potential for K⁺. Importantly, the currents produced by the Cybercyte I_{Kv12} model reliably reproduce the CX4-sensitive currents measured in action potential–clamp recordings from WT SCN neurons (Fig. S2 C).A Markov model describing the gating of the K⁺ channels that generate the A-current (I_A) was also developed using MATLAB (MathWorks Inc; Scheme 2). The model, which is based on a previously described model of the rapidly activating and inactivating K⁺ current in (ferret) ventricular myocytes, consists of three closed states, C_1–C_3, two inactivated states, I_O and I_1, and an open (O) state (Campbell et al., 1993), and was populated using acquired voltage-clamp data detailing the time- and voltage-dependent properties of I_A in mouse SCN neurons (Hermanstyne et al., 2017).
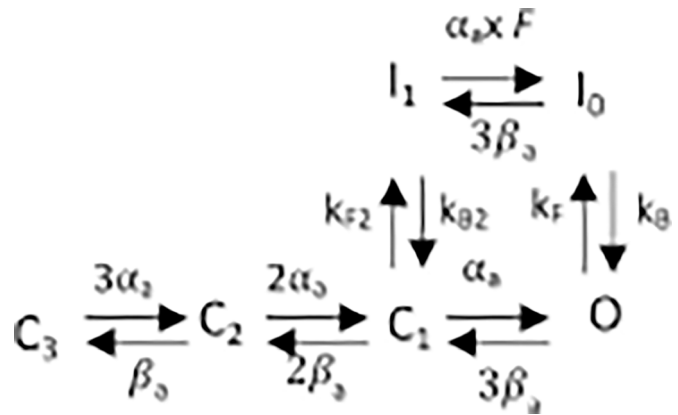
Scheme 2

The voltage-dependent transition rates for I_A activation and deactivation, α and β, respectively, determined from analyses of the time constants and sigmoidicity of I_A activation in SCN neurons (Hermanstyne et al., 2017), were $p_1\exp(p_2V_m)$ and $p_3\exp(-p_2V_m)$, respectively, where V_m is the membrane voltage, $p_1 = 0.5$, $p_2 = 0.0328$, and $p_3 = 0.0680$. In contrast to activation, the time constants of I_A inactivation in mouse SCN neurons were voltage independent over a wide range of membrane potentials (Hermanstyne et al., 2017). This finding suggests a "ball and chain" inactivation mechanism in which a putative "inactivation particle" interacts with the open channel to cause inactivation (Zagotta et al., 1990). In the I_A model, this inactivated state is I_O, and k_F, the voltage-insensitive "on" rate for the particle, is equal to the reciprocal of the inactivation time constant at positive potentials. The unbinding rate of the inactivation particle, k_B, was initially estimated by the ability of the model to match steady-state inactivation data for I_A (Aldrich et al., 1983). Such a single-state ball and chain model recovers very slowly from inactivation when the membrane is returned to hyperpolarized potentials. To account for the voltage-insensitive inactivation of I_A with relatively rapid recovery from inactivation, as observed experimentally (Hermanstyne et al., 2017), we introduced a transition state, I_1, into the model. In contrast to I_O, the I_1 state is a low-affinity binding state in which the energy from the backward movement of the voltage sensor during recovery destabilizes the binding interaction with the inactivation particle in a "push-off ball and chain" inactivation mechanism (Aldrich et al., 1983). The voltage-independent transition rates, k_F (0.05), k_B (0.00025), k_{F2} (0.05), and k_{B2} (0.002), were determined by fitting the data describing steady-state inactivation of I_A, and the experimentally determined time constants of I_A inactivation and recovery (at –70 mV) from inactivation (Hermanstyne et al., 2017). The ratio factor, F (8), was determined by macroscopic reversibility. The steady-state voltage-dependences of activation and inactivation of the modeled I_A are illustrated in Fig. S3 B. The currents are calculated as $I_A = G*P(O)*(V_m - E_K)$, where G is a scalable parameter for current magnitude, P(O) is the probability that the channel is open, and E_K is the reversal potential of K⁺. As also illustrated in Fig. S3, the simulated I_A waveforms evoked in response to depolarizing voltage steps (Fig. S3 C) are

Hermanstyne et al.
Kv12 channels regulate nighttime SCN neuronal firing

Journal of General Physiology   5 of 23
https://doi.org/10.1085/jgp.202213310

similar to I_A waveforms recorded from WT SCN neurons (Fig. S3 A).

A dynamic clamp was carried out using a commercially available Cybercyte Dynamic Clamp System, Cybercyte DC1 (Bett et al., 2013; Du et al., 2021) from Cytocybernetics. This system consists of a 16-channel, 16-bit, 100 kS/s MCC PCIe-DAS1602/16 board installed and configured in a Dell 5820 Precision workstation. The average loop time determined for this system was 22 µs. Prior to experiments on SCN neurons, the I_{K12} and I_A formulations were converted to Cybercyte channel definition files using Cybersolver software and validated by applying the simulated currents to a model cell (Molecular Devices) with an input resistance of 500 MΩ and a capacitance of 30 pF in whole-cell mode. The Cybercyte DC1 system allows current amplitudes to be scaled during dynamic clamp experiments such that the modeled currents (I_{K12} and I_A) can be "added" or "subtracted" (by the addition of I_{K12} or I_A of the opposite polarity) in real-time during whole-cell current-clamp recordings from nighttime and daytime WT SCN neurons.

Initial experiments were undertaken on nighttime WT SCN neurons to determine the minimal subtracted I_{Kv12} amplitude that increased the spontaneous repetitive firing rates of most (9 of 10) cells. These experiments revealed that the minimal subtracted (peak) I_{Kv12} amplitude required to affect repetitive firing rates in most (9 of 10) nighttime WT SCN neurons was 2 pA, and this value was set as x. The effects of subtracting varying amplitudes (in integral multiples of x) of I_{Kv12} on the repetitive firing rates of WT nighttime neurons were then determined. For daytime WT neurons, I_{Kv12} was scaled (to 0.5 pA) to reflect the day–night difference in the (mean) CX4-sensitive current amplitudes measured in WT neurons (Fig. 4 D), and the effects of the subtraction of integral multiples of this value (i.e., x = 0.5 pA) on the repetitive firing rates of daytime WT neurons were determined. A similar strategy was used in dynamic clamp experiments to determine the effects of adding I_{Kv12} in nighttime and daytime WT neurons, as well as of subtracting/adding I_A in nighttime and daytime WT SCN neurons. Preliminary experiments revealed that the minimal added I_{Kv12} amplitude required to affect repetitive firing rates in most (9 of 10) nighttime WT SCN neurons was 5 pA and I_{Kv12} was scaled (to 2 pA), again to reflect the day–night difference in CX4-sensitive current amplitudes measured in WT neurons (Fig. 4 D). The minimal modeled I_A amplitude required to alter repetitive firing rates in most (9 of 10) nighttime WT SCN neurons was 20 pA. In addition, because previous studies demonstrated that I_A densities in WT nighttime and daytime SCN neurons are not significantly different (Hermanstyne et al., 2017), no day–night scaling factor was used.

For dynamic clamp recordings, the membrane voltage was sampled at 20 kHz and the Cybercyte DC1 returned the corresponding modeled I_{Kv12} (or I_A) at a rate of 50 kHz. For each cell, spontaneous repetitive firing was recorded for 1 min. Modeled currents were then added or subtracted in multiples (i.e., x, 2x, −x, −2x, etc.) of the minimal (x) amplitudes, determined as described above, and the resulting repetitive firing rates were measured. The percent change in the repetitive firing rate with each current injection was then determined in each cell. These values were then averaged across cells and the mean ± SEM percent changes in firing rates as a function of the injected current amplitudes are presented.

Analyses of wheel-running activity

Adult (9–12 wk old) WT, Kv12.1$^{−/−}$, Kv12.2$^{−/−}$, and DKO mice were placed (individually) in cages equipped with running wheels in light-tight chambers illuminated with fluorescent bulbs (2.4 ± 0.5 × 10^{18} photons/s*m^2; General Electric). Wheel-running activity was recorded (Clocklab Actimetrics) in 6-min bins for 10 d in a 12:12 h LD cycle, followed by recordings in constant darkness (DD) for at least 20 d. Similar recordings were obtained from animals 10 d following bilateral injections (600 nl in each hemisphere) of the NT, Kv12.1-targeted, or Kv12.2-targeted shRNA-expressing AAV8 into the SCN of adult (9–12 wk) WT mice. The period of rhythmicity of each mouse was determined using χ^2 periodogram analysis (Sokolove and Bushell, 1978) of continuous recordings for 10 d in DD (Clocklab Actimetrics). Wheel-running was considered rhythmic if the χ^2 periodogram value exceeded the 99.9% confidence interval (Qp value). Statistical analysis of the circadian periods was compared between groups using a one-way analysis of variance (ANOVA).

Quantitative RT-PCR analysis

Total RNA was isolated from (300 µm) SCN slices, collected every 4 h (ZT 3, 7, 11, 15, 19, and 23) for two consecutive days from adult (8–10 wk) WT mice (n = 7–8), maintained in standard and reversed LD conditions, and DNase treated using previously described methods (Marionneau et al., 2008). RNA concentrations were determined by optical density measurements (Marionneau et al., 2008). The mRNA transcript expression levels of genes encoding *Per2*, *Bmal*, *Kcnh8* (Kv12.1), *Kcnh3* (Kv12.2), as well as of the endogenous control gene *Hprt* (hypoxanthine guanine phosphoribosyl transferase), were determined using Taqman-based real-time quantitative (RT) PCR. Data were collected with instrument spectral compensations using the Applied Biosystems SDS 2.2.2 software and analyzed using the threshold cycle (C_T) relative quantification method (Schmittgen and Livak, 2008). The expression of each transcript was normalized to the expression of *Hprt* in the same sample and evaluated for rhythmicity using JTK cycle analysis (Hughes et al., 2010) with the period set to 24 h. The primers sequences used were *Per2*: 5′-TCCACCGGCTACTGATGCA-3′ and 5′-TGGATGATGTCTGGCTCATGA-3′; *Bmal*: 5′-GTAGGATGTGACCGAGGGAAGA-3′ and 5′-AGTCAAACAAGCTCTGGCCAAT-3′; *Kcnh8* (Kv12.1): 5′-AGGATTACTGGCGCCACAGA-3′ and 5′-CTTTGCCACTTGGGCATTG-3′; *Kcnh3* (Kv12.2): 5′-GCAACGTGTCCGCTAACACA-3′ and 5′-GCCGTCACATTCCCAAACA-3′; and *Hprt*: 5′-TGAATCACGTTTGTGTCATTAGTGA-3′ and 5′-TTCAACTTGCGCTCATCTTAGG-3′.

Statistical analysis

Electrophysiological data were compiled and analyzed using ClampFit (v. 10.2; Molecular Devices), Mini Analysis (v. 6.0.7; Synaptosoft), and Prism (v. 8.2; GraphPad Software). Averaged data are presented as means ± standard error of the means (SEM). Statistical analyses were performed using Student's t test

or one-way ANOVA with Newman-Kuels post-hoc pairwise comparisons, as indicated in the text, figure legends, or tables; P values are reported.

Online supplemental material

Fig. S1 illustrates the strategy used to generate Kv12.1$^{-/-}$ mouse line, together with the validation of this mouse line. Fig. S2 shows the waveforms of the CX4-sensitive K$^+$ currents in WT SCN neurons and the Cybercyte modeled Kv12 currents, I$_{Kv12}$, and Fig. S3 shows the Cybercyte modeled I$_A$. In Fig. S4, the average repetitive firing rates and membrane properties determined in individual SCN slices from WT, Kv12.1$^{-/-}$, Kv12.2$^{-/-}$, NT shRNA-expressing, Kv12.1 shRNA-expressing, and Kv12.2 shRNA expressing animals are shown. The repetitive firing rates determined in WT, Kv12.1$^{-/-}$, and Kv12.2$^{-/-}$ SCN neurons throughout the day and night are presented in Fig. S5. The effects of the dynamic clamp-mediated addition of I$_{Kv12}$ on the repetitive firing rates of nighttime WT and Kv12.1$^{-/-}$ SCN neurons are compared in Fig. S6. The kinetic differences between the modeled I$_A$ and I$_{Kv12}$ are illustrated in Fig. S7 and, in Fig. S8, the effects of dynamic clamp-mediated subtraction of I$_A$ and I$_{Kv12}$ versus I$_A$ are compared directly. In Fig. S9, the variations in the transcript expression levels of *Kcnh8* (Kv12.1), *Kcnh3* (Kv12.2), as well as of *Per* and *Bmal*, measured over a 48-h period at 4-h intervals, are presented. Table S1 presents the data represented in Fig. S4.
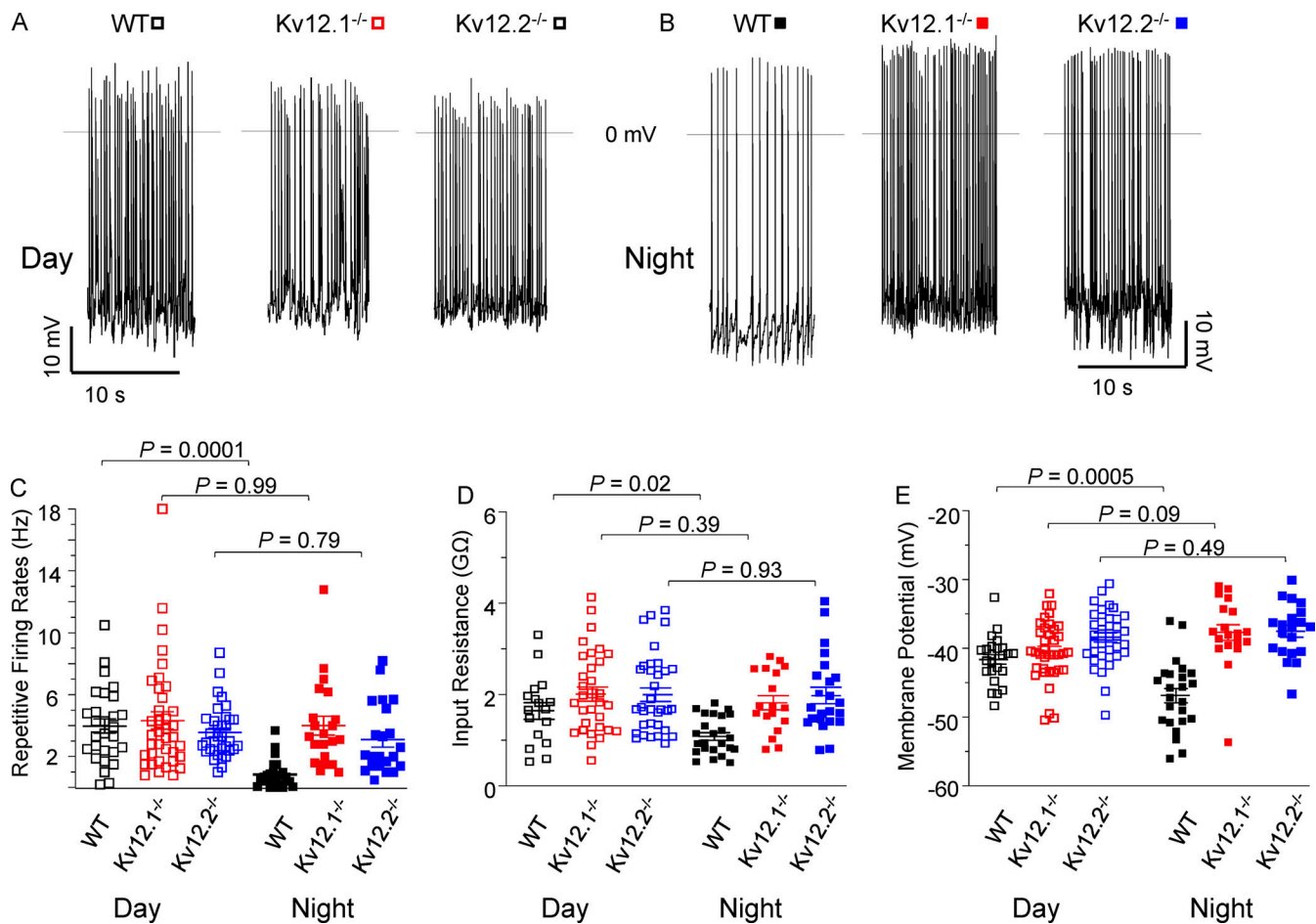
Results

Targeted deletion of Kcnh8 or Kcnh3 selectively alters nighttime firing rates in SCN neurons

To explore the roles of Kv12.1/Kv12.2-encoded K$^+$ channels in regulating spontaneous repetitive firing in the SCN, we obtained whole-cell current-clamp recordings during the day (ZT7–ZT12) and at night (ZT19–ZT24) from SCN neurons in slices prepared from adult WT mice and from animals harboring targeted disruptions in the *Kcnh8* (Kv12.1$^{-/-}$) or the *Kcnh3* (Kv12.2$^{-/-}$) locus (Fig. 1). Representative recordings from daytime (Fig. 1 A) and nighttime (Fig. 1 B) WT, Kv12.1$^{-/-}$, and Kv12.2$^{-/-}$ SCN neurons are shown in Fig. 1. Consistent with previous reports (Brown and Piggins, 2007; Allen et al., 2017; Belle and Allen, 2018; Harvey et al., 2020), these experiments revealed a large (P = 0.0001, one-way ANOVA) day–night difference in the mean ± SEM repetitive firing rates of WT SCN neurons (Fig. 1 C and Table 1). In marked contrast, there were no measurable differences in the mean ± SEM daytime and nighttime repetitive firing rates of Kv12.1$^{-/-}$ (P = 0.99, one-way ANOVA) or Kv12.2$^{-/-}$ (P = 0.79, one-way ANOVA) SCN neurons (Fig. 1 C and Table 1). In addition, the loss of the day–night difference in the mean repetitive firing rates of Kv12.1$^{-/-}$ and Kv12.2$^{-/-}$ SCN neurons reflects a selective increase (compared with WT cells) in mean nighttime repetitive firing rates (Fig. 1 C and Table 1); the daytime repetitive firing rates of Kv12.1$^{-/-}$ and Kv12.2$^{-/-}$ SCN neurons are similar to WT cells (Fig. 1 C and Table 1). Similar results were obtained in recordings from SCN neurons in slices prepared from Kv12.1$^{-/-}$/Kv12.2$^{-/-}$ (DKO) animals lacking both Kv12.1 and Kv12.2.

As is evident in Fig. 1 C, the repetitive firing rates of WT, as well as Kv12.1$^{-/-}$ and Kv12.2$^{-/-}$, SCN neurons are quite variable. Similar variability in (in daytime and nighttime) repetitive firing rates for all genotypes was evident across slices/animals. Importantly, comparisons of the averaged data acquired in individual animals (N; Fig. S4) also revealed a large (P = 0.0001, one-way ANOVA) day–night difference in the mean repetitive firing rates in WT SCN slices (Fig. S4 A and Table S1), whereas there were no day–night differences in mean repetitive firing rates determined in SCN slices prepared from Kv12.1$^{-/-}$ (P = 0.84, one-way ANOVA) or Kv12.2$^{-/-}$ (P = 0.55, one-way ANOVA) animals (Fig. 1 C, Table 1, Fig. S4, and Table S1).

Also consistent with previous reports (Brown and Piggins, 2007; Allen et al., 2017; Belle and Allen, 2018; Harvey et al., 2020), there were marked day–night differences in the mean ± SEM input resistances (Fig. 1 D; P = 0.02, one-way ANOVA), resting membrane potentials (Fig. 1 E; P = 0.0005, one-way ANOVA), and interspike intervals (Table 1; P = 0.001, one-way ANOVA) of WT SCN neurons (Table 1). In contrast, the mean ± SEM input resistances, resting membrane potentials, and interspike intervals measured in daytime and nighttime Kv12.1$^{-/-}$, Kv12.2$^{-/-}$, or DKO SCN neurons were not significantly different (Fig. 1, D and E; and Table 1). Similar results were obtained when the average data acquired in SCN slices from individual animals were compared (Fig. S4 and Table S1). Consistent with the repetitive firing data, these results reflect the higher mean input resistances and depolarized membrane potentials of nighttime Kv12.1$^{-/-}$, Kv12.2$^{-/-}$, and DKO compared with nighttime WT, SCN neurons (Fig. 1, D and E; Table 1; and Table S1). The mean ± SEM daytime input resistances and resting membrane potentials of Kv12.1$^{-/-}$, Kv12.2$^{-/-}$, and DKO SCN neurons are similar to those measured in daytime WT SCN neurons (Fig. 1, D and E; and Table 1).

Because the majority of the data presented in Fig. 1 and Table 1 was obtained during the latter portion of the night (i.e., ZT20–ZT24), additional recordings were obtained throughout the light–dark cycle. Specifically, additional cell-attached current-clamp recordings were obtained from cells in slices during the transition from lights-on to lights-off (ZT12–ZT14), as well as slices prepared mid-day (ZT6–ZT8) and mid-evening (ZT18–ZT20). Analysis of these recordings revealed that during the transition from day to night, the mean repetitive firing rate of WT SCN neurons decreased to ∼1 Hz (compared to ∼4 Hz at mid-day), and this rate was maintained to the end of the night phase (Fig. S5). In marked contrast, the mean repetitive firing rates of Kv12.1$^{-/-}$ and Kv12.2$^{-/-}$ SCN neurons during the "day to night" transition (∼3.5 Hz) were much higher (Fig. S5) and remained high at midday and mid-evening (Fig. S5). In addition, the mean ± SEM daytime repetitive firing rates of Kv12.1$^{-/-}$ and Kv12.2$^{-/-}$ SCN neurons are indistinguishable from WT SCN cells (Fig. 1 C and Table 1). Similar results were obtained in recordings from DKO SCN neurons (Table 1). Consistent with the similarities in repetitive firing rates measured during the day and at night, Kv12.1$^{-/-}$, Kv12.2$^{-/-}$, and DKO SCN neurons do not display the day–night difference in interspike intervals characteristic of WT SCN neurons (Table 1). Taken together, these results demonstrate that the repetitive firing

Figure 1. **The repetitive firing rates of Kv12.1$^{-/-}$ and Kv12.2$^{-/-}$ SCN neurons are similar during the day and at night. (A and B)** Representative daytime (A) and nighttime (B) whole-cell current-clamp recordings from WT (black squares), Kv12.1$^{-/-}$ (red squares), and Kv12.2$^{-/-}$ (blue squares) SCN neurons are shown. **(C)** Daytime and nighttime repetitive firing rates, measured in individual WT (black squares), Kv12.1$^{-/-}$ (red squares), and Kv12.2$^{-/-}$ (blue squares) SCN neurons are plotted; mean ± SEM repetitive firing rates are indicated; n = numbers of cells. As reported previously (Brown and Piggins, 2007; Allen et al., 2017; Belle and Allen, 2018; Harvey et al., 2020), the mean ± SEM repetitive firing rate in WT SCN neurons is higher (P = 0.0001, one-way ANOVA) during the day than at night (Table 1). In contrast, there are no day–night differences (one-way ANOVA) in the mean ± SEM repetitive firing rates of Kv12.1$^{-/-}$ (red squares; P = 0.99) or Kv12.2$^{-/-}$ (blue squares; P = 0.79) SCN neurons (Table 1). **(D and E)** Input resistances (D) and membrane potentials (E), measured in individual WT (black squares), Kv12.1$^{-/-}$ (red squares), and Kv12.2$^{-/-}$ (blue squares) SCN neurons during the day and at night, are plotted; mean ± SEM values and P values are indicated. In contrast to WT SCN neurons, there are no day–night differences (one-way ANOVA) in the mean ± SEM input resistances (D) or membrane potentials (E) of Kv12.1$^{-/-}$ (red squares) or Kv12.2$^{-/-}$ (blue squares) SCN neurons (Table 1).

rates of Kv12.1$^{-/-}$ and Kv12.2$^{-/-}$ SCN neurons are increased throughout the night.

Acute in vivo knockdown of Kv12.1 or Kv12.2 also selectively increases nighttime firing rates

The electrophysiological studies above demonstrate increased repetitive firing rates and input resistances, reduced interspike intervals, and depolarized resting membrane potentials in nighttime Kv12.1$^{-/-}$, Kv12.2$^{-/-}$, and DKO, compared with WT, SCN neurons; the repetitive firing and intrinsic membrane properties of daytime Kv12.1$^{-/-}$, Kv12.2$^{-/-}$, DKO, and WT SCN neurons, in contrast, are indistinguishable (Fig. 1, Fig. S4, Table 1, and Table S1). Interpreting the physiological significance and the functional implications of these findings is confounded, however, by the fact that the Kv12.1$^{-/-}$, Kv12.2$^{-/-}$, and DKO mice lack Kv12.1 or/and Kv12.2 throughout development. Additional

experiments were undertaken, therefore, to test the hypotheses that Kv12.1 and/or Kv12.2 are required for the regulation of the nighttime repetitive firing rates and the membrane properties of mature SCN neurons using an interfering RNA (Du et al., 2006) strategy to knockdown the expression of the Kv12.1 and Kv12.2 subunits acutely in the SCN of adult animals in vivo.

To identify shRNA sequences that effectively reduce Kv12.1 (or Kv12.2) expression, five Kv12.1-targeted (or five Kv12.2-targeted) shRNAs were screened individually in tsA-201 cells cotransfected with a cDNA construct encoding Kv12.1-eYFP (or Kv12.2-eYFP). The Kv12.1-targeted (and Kv12.2-targeted shRNA) sequences providing the maximal (~80%) reductions in Kv12.1 (or Kv12.2) expression identified in these initial screens (see Materials and methods) were further evaluated for specificity. In these experiments, tsA-201 cells were cotransfected with the validated Kv12.1-targeted or Kv12.2-targeted shRNA or a NT

Table 1. Resting and active membrane properties of WT, Kv12.1$^{-/-}$, Kv12.2$^{-/-}$, and DKO (Kv12.1$^{-/-}$/Kv12.2$^{-/-}$) SCN neurons during the day and at night

		Firing rate (Hz)	R_{in} (GΩ)	V_r (mV)	ISI (ms)
Day ZT 7–12	WT	4.0 ± 0.5 n = 28	1.7 ± 0.2** n = 20	−41.6 ± 0.7*** n = 28	280 ± 9* n = 28
	Kv12.1$^{-/-}$	4.3 ± 0.6 n = 38	2.0 ± 0.2 n = 33	−40.4 ± 0.7 n = 38	252 ± 9 n = 38
	Kv12.2$^{-/-}$	3.6 ± 0.3 n = 35	2.0 ± 0.1 n = 34	−38.4 ± 0.7 n = 35	311 ± 9 n = 35
	DKO	4.1 ± 0.3 n = 6	1.6 ± 0.2 n = 6	−40.8 ± 1.6 n = 6	279 ± 13 n = 6
Night ZT 18–24	WT	0.8 ± 0.2* n = 25	1.0 ± 0.1** n = 24	−46.7 ± 1.0*** n = 25	418 ± 29* n = 20
	Kv12.1$^{-/-}$	4.0 ± 0.7 n = 21	1.8 ± 0.2 n = 18	−37.7 ± 1.2 n = 21	254 ± 6 n = 21
	Kv12.2$^{-/-}$	3.1 ± 0.5 n = 22	2.0 ± 0.2 n = 22	−37.5 ± 0.9 n = 22	319 ± 17 n = 22
	DKO	3.4 ± 0.4 n = 6	1.5 ± 0.2 n = 6	−40.5 ± 3.2 n = 6	318 ± 12 n = 6

Values are means ± SEM; n = number of cells; R_{in} = input resistance; V_r = resting membrane potentials; ISI = interspike interval. Values in daytime and nighttime WT neurons are significantly different (*P = 0.0001; **P = 0.02; ***P = 0.0005).

shRNA with cDNA constructs encoding Kv12.1-eYFP, Kv12.2-eYFP, or Kv4.1-eYFP (from another Kv subfamily). As illustrated in Fig. 2, Western blot analysis revealed that the Kv12.1-targeted shRNA markedly reduced the expression of Kv12.1-eYFP (Fig. 2 A), without measurably affecting Kv12.2-eYFP or Kv4.1-eYFP (Fig. 2, B and C). Similarly, the Kv12.2-targeted shRNA markedly reduced Kv12.2-eYFP, without measurably affecting Kv12.1-eYFP or Kv4.1-eYFP (Fig. 2, A–C). These selective Kv12.1-targeted and Kv12.2-targeted shRNAs, as well as the NT shRNA, were then cloned (separately), in a microRNA (human miR30) context (Stegmeier et al., 2005), into a plasmid containing a synapsin promoter and eGFP (Hermanstyne et al., 2017), and adeno-associated viruses serotype 8 (AAV8) were generated.

2 wk following stereotaxic injections of the Kv12.1-targeted, Kv12.2-targeted, or NT shRNA-expressing AAV8 into the adult SCN, whole-cell current-clamp recordings were obtained from eGFP-positive SCN neurons in slices (Fig. 2 D). Representative recordings from NT, Kv12.1-targeted, and Kv12.2-targeted shRNA-expressing SCN neurons during the daytime (ZT7–ZT12) and nighttime (ZT18–ZT24) are presented in Fig. 3, A and B. Analyses of the repetitive firing data acquired from many daytime and nighttime eGFP-positive SCN neurons revealed a day–night difference in the mean ± SEM repetitive firing rates of NT shRNA-expressing SCN neurons (Fig. 3 C and Table 2). Similar to WT neurons (Table 1), the mean ± SEM repetitive firing rate measured in NT shRNA-expressing SCN neurons was much (P = 0.0001, one-way ANOVA) higher during the day than at night (Fig. 3 C and Table 2). In contrast, the mean ± SEM repetitive firing rates of both Kv12.1-targeted shRNA- (P = 0.11) and Kv12.2-targeted (P = 0.84) shRNA-expressing SCN neurons were similar day and night. The lack of day–night differences in the mean ± SEM repetitive firing rates of Kv12.1-targeted and

Kv12.2-targeted shRNA-expressing SCN neurons reflects the fact that the nighttime firing rates in these cells were high compared with nighttime NT shRNA-expressing SCN neurons (Fig. 3 C and Table 2).

Similar to the results obtained in WT, Kv12.1$^{-/-}$, and Kv12.2$^{-/-}$ slices, the repetitive firing rates measured in daytime and nighttime NT, Kv12.1-targeted, and Kv12.2-targeted shRNA-expressing SCN neurons are quite variable. Similar variability in (in daytime and nighttime) repetitive firing rates was also evident across slices/animals, and comparisons of the averaged data acquired in individual slices (Fig. S4) revealed a marked (P = 0.01, one-way ANOVA) day–night difference in the mean repetitive firing rates measured in slices prepared from NT shRNA-expressing animals (Fig. S4 D and Table S1), whereas there were no day–night differences in mean repetitive firing rates determined in SCN slices prepared from Kv12.1-targeted (P = 0.18, one-way ANOVA) or Kv12.2-targeted (P = 0.64, one-way ANOVA) shRNA-expressing animals (Fig. S4 and Table S1).

Similar to WT SCN neurons (Table 1), input resistances were higher (P = 0.0001, one-way ANOVA), resting membrane potentials were more depolarized (P = 0.004, one-way ANOVA), and interspike intervals were shorter (P = 0.0001, one-way ANOVA) in NT shRNA-expressing SCN neurons during the day than at night (Fig. 3, D and E; and Table 2). In contrast, the input resistances, resting membrane potentials, and interspike intervals measured in Kv12.1-targeted and Kv12.2-targeted shRNA-expressing SCN neurons (P = 0.93, one-way ANOVA) at night and during the day were similar (Fig. 3, D and E; and Table 2). Similar results were obtained when the average data acquired in SCN slices from individual NT, Kv12.1-targeted, and Kv12.2-targeted shRNA-expressing SCN animals were compared (Fig. S4 and Table S1). The functional effects of the acute in vivo
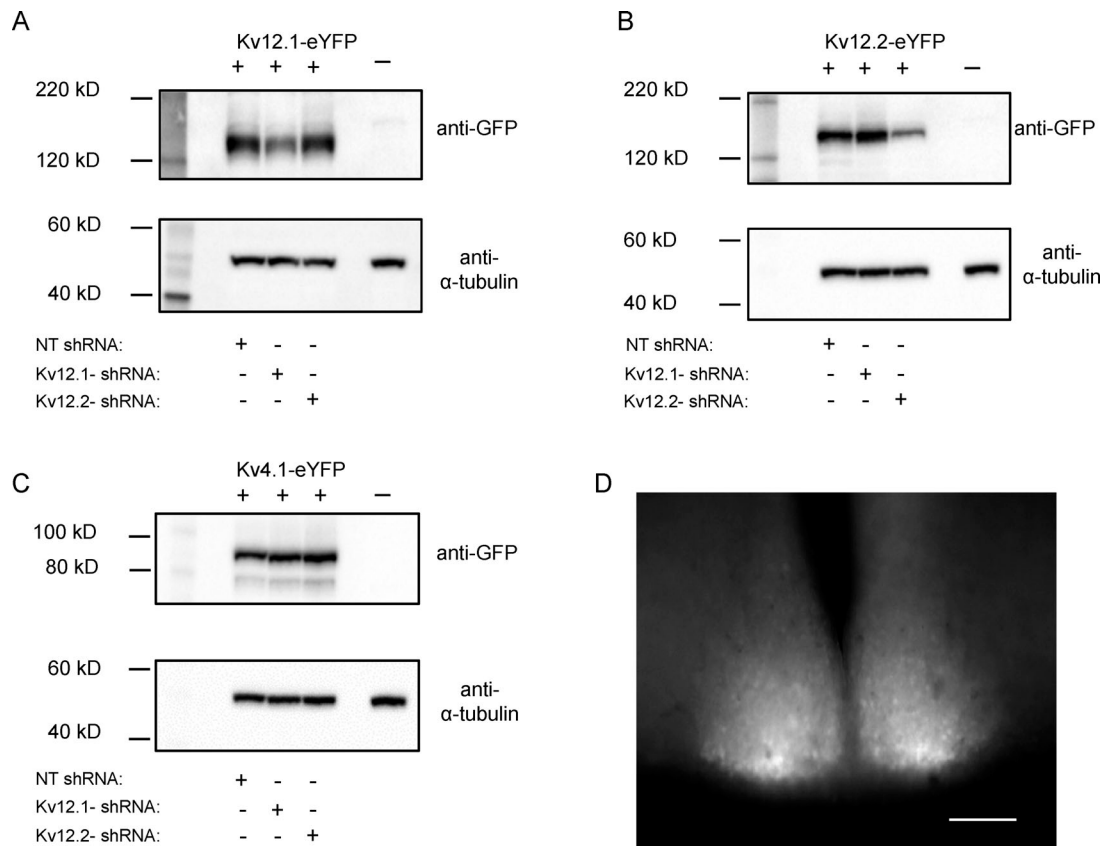
Hermanstyne et al.
Kv12 channels regulate nighttime SCN neuronal firing

Journal of General Physiology   9 of 23
https://doi.org/10.1085/jgp.202213310

Figure 2. Validation of the Kv12.1-targeted and Kv12.2-targeted shRNAs. To examine the specificity of the selected Kv12.1-targeted and Kv12.2-targeted shRNAs, each was expressed in tsA-201 cells with a cDNA construct encoding Kv12.1-eYFP, Kv12.2-eYFP, or Kv4.1-eYFP; parallel experiments were completed with the NT shRNA. Approximately 24 h following transfections, cell lysates were prepared, fractionated by SDS-PAGE, transferred to PVDF membranes, and probed with an anti-GFP antibody. All blots were also subsequently probed with an anti-α-tubulin antibody to verify equal protein loading. **(A)** Co-expression with the Kv12.1-targeted shRNA markedly reduced Kv12.1-eYFP protein expression, whereas the Kv12.2-targeted shRNA and the NT shRNA were without effects on Kv12.1-eYFP. **(B)** Similarly, co-expression with the Kv12.2-targeted shRNA, but not the Kv12.1-targeted or the NT shRNA, reduced Kv12.2-eYFP protein expression. **(C)** In contrast, neither the Kv12.1-targeted nor the Kv12.2-targeted shRNA measurably affected expression of Kv4.1-eYFP. The complete blots from which the "cut outs" shown in A–C were derived are provided in the source data. **(D)** eGFP-expressing neurons were readily identified in acute SCN slices prepared 2 wk following bilateral injections of the Kv12.1-targeted (or the Kv12.2-targeted) shRNA-expressing AAV8 into the SCN; scale bar = 250 µm. Source data are available for this figure: SourceData F2.

knockdown of Kv12.1 or Kv12.2 (Table 2 and Table S1) on the repetitive firing rates and membrane properties of SCN neurons, therefore, are virtually identical to those observed in Kv12.1$^{-/-}$ and Kv12.2$^{-/-}$ (Table 1 and Table S1) SCN neurons (see Discussion).

Kv12-encoded current densities are higher in nighttime, than in daytime, SCN neurons

The selective effects of the targeted deletion or the acute knockdown of Kv12.1 or Kv12.2 on the nighttime repetitive firing rates and membrane properties of SCN neurons suggest day–night differences in the functional expression of Kv12-encoded K$^+$ currents. To explore this hypothesis directly, whole-cell voltage-clamp recordings were obtained from daytime and nighttime WT and DKO SCN neurons before and after the application of 20 µM CX4, reported to be a selective blocker of heterologously expressed Kv12.2-encoded K$^+$ currents (Zhang et al., 2010). In these experiments, whole-cell outward K$^+$ currents, evoked in response to action potentials waveforms (Fig. 4

A) obtained from nighttime WT SCN neurons, were recorded from daytime and nighttime WT (Fig. 4 B) and DKO (Fig. 4 C) SCN neurons with TTX and CdCl$_2$ in the bath to block voltage-gated Na$^+$ and Ca^{2+} channels, respectively. Offline digital subtraction of the currents recorded before and after exposure to CX4 provided the CX4-sensitive outward K$^+$ currents. As is evident in the representative recordings shown in Fig. 4 B, the density of the CX4-sensitive K$^+$ current is higher in the nighttime, compared with the daytime, WT SCN neuron. Similar results were obtained in recordings from multiple WT neurons (Fig. 4 D). The mean ± SEM CX4-sensitive current densities measured in daytime and nighttime WT SCN neurons were 7.9 ± 1.8 pA/pF ($n = 17$) and 23.6 ± 6.3 pA/pF ($n = 13$), respectively. The marked day–night difference in the densities of the CX4-sensitive outward K$^+$ currents observed in WT SCN neurons, however, is not evident in DKO SCN neurons (Fig. 4 C). However, there are residual CX4-sensitive currents in DKO SCN neurons (Fig. 4 D), and the mean ± SEM CX4-sensitive outward K$^+$ current densities measured in daytime and nighttime DKO
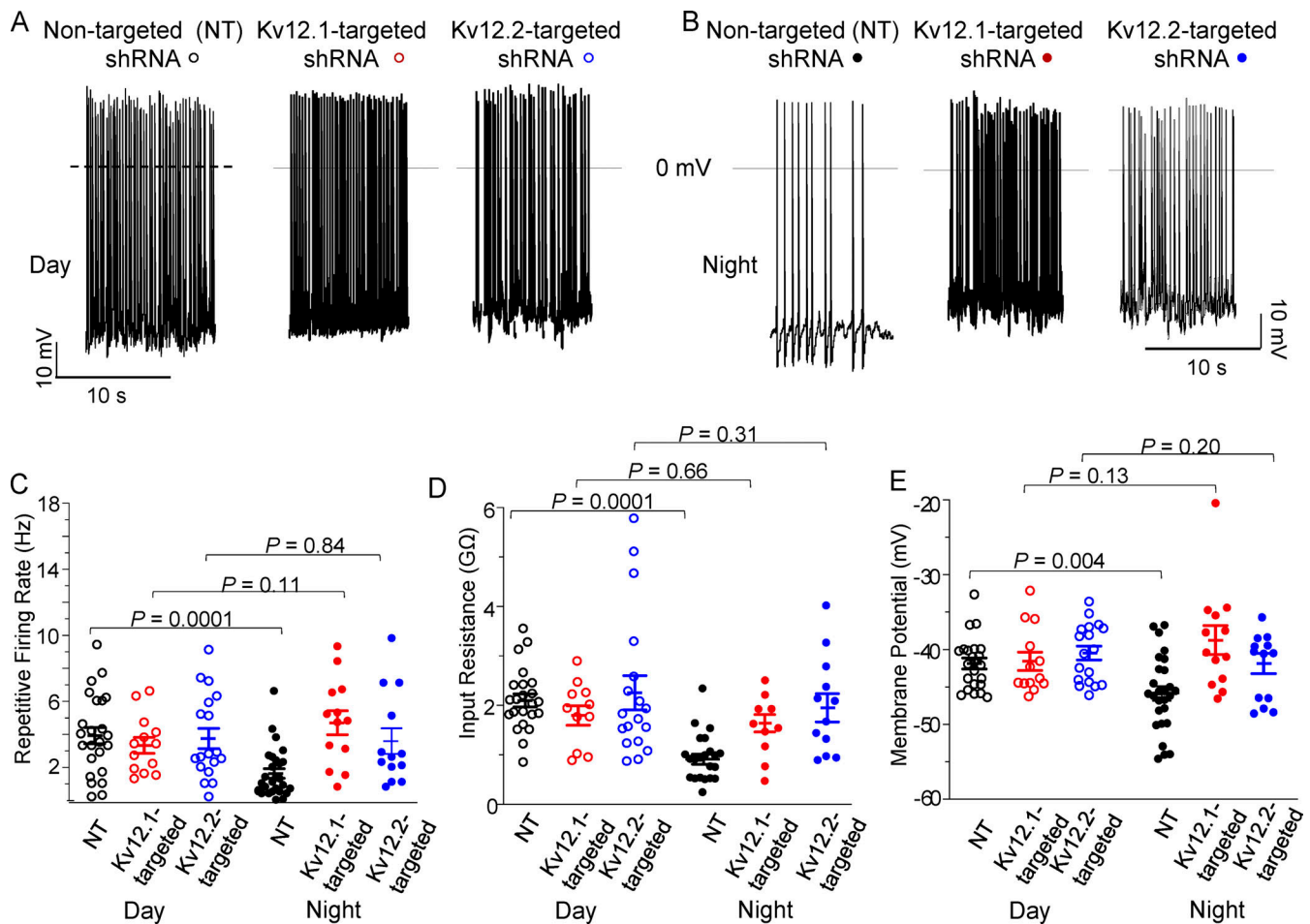
Figure 3. **Acute in vivo shRNA-mediated knockdown of Kv12.1 or Kv12.2 increases the nighttime, but not the daytime, repetitive firing rates of SCN neurons. (A and B)** Representative daytime (A) and nighttime (B) whole-cell current-clamp recordings obtained from NT shRNA- (black circles), Kv12.1-targeted shRNA- (red circles), and Kv12.2-targeted shRNA- (blue circles) expressing SCN neurons during the day (ZT7–ZT12) and at night (ZT18–ZT24) are shown. **(C)** Daytime and nighttime repetitive firing rates measured in individual SCN neurons expressing the NT (black circles), Kv12.1-targeted (red circles), or Kv12.2-targeted shRNA (blue circles) are plotted; mean ± SEM repetitive firing rates are indicated. Similar to WT SCN[7–10] neurons (Fig. 1), the mean ± SEM repetitive firing rate of NT shRNA-expressing (black circles) SCN neurons was lower (P = 0.0001, one-way ANOVA) at night than during the day (Table 2). In marked contrast, the mean ± SEM repetitive firing rates of Kv12.1- (red circles) and Kv12.2- (blue circles) targeted shRNA-expressing SCN neurons at night are not (one-way ANOVA) different from daytime firing rates (Table 2). **(D and E)** The input resistances (D) and membrane potentials (E) of NT shRNA- (black circles), Kv12.1-targeted shRNA- (red circles), and Kv12.2-targeted shRNA-expressing (blue circles) SCN neurons during the day and at night were also determined. Similar to WT SCN neurons[7–10], the mean ± SEM input resistance of NT shRNA-expressing (black circles) SCN neurons was higher (P = 0.0001, one-way ANOVA) during the day than at night, and the mean ± SEM membrane potential was more depolarized (P = 0.004, one-way ANOVA), during the day than at night (Table 2). In contrast, there were no day–night differences (one-way ANOVA) in the mean ± SEM input resistances (D) or membrane potentials (E) of Kv12.1-targeted shRNA- (red circles) and Kv12.2-targeted shRNA-expressing (blue circles) SCN neurons (Table 2).

SCN neurons were statistically indistinguishable at 4.3 ± 1.2 pA/pF ($n = 8$) and 5.6 ± 1.3 pA/pF ($n = 8$), respectively (Fig. 4 D). The densities of the residual CX4-sensitive outward K⁺ currents in daytime and nighttime DKO SCN neurons, therefore, are quite similar (see Discussion).

Although the action potential- (voltage-) clamp recordings (Fig. 4) reveal that the mean ± SEM CX4-sensitive outward K⁺ current density is considerably higher in nighttime than in daytime WT SCN neurons, there were a couple of daytime WT SCN neurons with higher than average CX4-sensitive current densities. In addition, the CX4-sensitive current densities measured in individual nighttime WT SCN neurons were quite variable (Fig. 4 D). To explore the functional consequences of

these apparent differences, the effects of CX4 on the repetitive firing properties of SCN neurons were examined in whole-cell current-clamp recordings from cells in acute slices prepared from WT animals during the day (ZT7–ZT12) or at night (ZT18–ZT24). Consistent with the action potential- (voltage-) clamp data (Fig. 4), these experiments revealed that the application of 20 μM CX4 increased repetitive firing rates in only a small fraction (2 of 17; ~10%) of daytime WT SCN neurons (Fig. 5 C), whereas the repetitive firing rates of most (11 of 15; ~70%) nighttime WT SCN neurons were increased following application of 20 μM CX4 (Fig. 5 D). In addition to confirming day–night differences in the functional expression of Kv12-encoded K⁺ currents, these observations suggest that there is cellular

Hermanstyne et al.
Kv12 channels regulate nighttime SCN neuronal firing

Journal of General Physiology
https://doi.org/10.1085/jgp.202213310

11 of 23

Table 2. Resting and active membrane properties of NT, Kv12.1-targeted, and Kv12.2-targeted shRNA-expressing SCN neurons during the day and at night

		Firing rate (Hz)	R_{in} (GΩ)	V_r (mV)	ISI (ms)
Day ZT 7–12	NT shRNA	3.9 ± 0.5* n = 24	2.1 ± 0.1 n = 23	−41.5 ± 0.7** n = 24	221 ± 4* n = 24
	Kv12.1-targeted shRNA	3.3 ± 0.5 n = 13	1.8 ± 0.2 n = 11	−41.5 ± 1.2 n = 13	213 ± 9 n = 13
	Kv12.2-targeted shRNA	3.8 ± 0.6 n = 18	2.3 ± 0.3 n = 18	−40.5 ± 0.9 n = 18	243 ± 8 n = 18
Night ZT 18–24	NT shRNA	1.6 ± 0.3* n = 27	0.9 ± 0.1* n = 22	−45.8 ± 1.0** n = 27	366 ± 24* n = 27
	Kv12.1-targeted shRNA	4.7 ± 0.7 n = 13	1.6 ± 0.2 n = 9	−38.7 ± 1.9 n = 13	187 ± 5 n = 13
	Kv12.2-targeted shRNA	3.6 ± 0.8 n = 13	1.9 ± 0.3 n = 12	−42.6 ± 1.5 n = 13	234 ± 6 n = 13

Values are means ± SEM; n = number of cells; R_{in} = input resistance; V_r = resting membrane potentials; ISI = interspike interval. Values in daytime and nighttime NT shRNA-expressing neurons are significantly (*P = 0.0001; **P < 0.004) different.

heterogeneity in the subthreshold K^+ channels mediating the day–night switch in the repetitive firing rates of SCN neurons (see Discussion).

Dynamic clamp-mediated subtraction of I_{Kv12} increases firing rate in nighttime WT SCN neurons

To explore the impact of changing Kv12-encoded current amplitudes on the spontaneous repetitive firing rates of SCN neurons directly, we employed dynamic clamps to manipulate the Kv12-encoded current (I_{Kv12}) electronically in real time during current-clamp recordings. As described in Materials and methods, a model of I_{Kv12} was developed using published data on heterologously expressed Kv12.1 currents (Engeland et al., 1998). The steady-state voltage-dependence of activation of I_{Kv12} in the model was then adjusted to fit the voltage- (Fig. S3, A and B) and action potential- (Fig. 4) clamp data acquired from WT SCN neurons. The properties and amplitudes of I_{Kv12} produced by the model (Fig. S3 C) reliably reproduce the CX4-sensitive currents identified in action potential-clamp recordings from WT SCN neurons.

In all dynamic clamp experiments, whole-cell current-clamp recordings were obtained from SCN neurons in acute slices prepared from adult WT animals at night or during the day. After recording gap-free spontaneous firing activity under control conditions (Fig. 6, A and E), the effects on spontaneous repetitive firing rates of subtracting or increasing I_{Kv12} amplitudes were determined. Initial experiments were conducted on nighttime WT SCN neurons to determine the minimal subtracted I_{Kv12} amplitude that increased the spontaneous repetitive firing rates of most (9 of 10) cells. These experiments revealed that the minimal (peak) amplitude of I_{Kv12} amplitude that increased the repetitive firing rates of most (9 of 10) nighttime WT SCN neurons was 2 pA. This value (2 pA) was then set equal to x, and the effects of subtracting varying amplitudes (in integral multiples of x) of I_{Kv12} on the repetitive firing rates of WT nighttime neurons were determined. For daytime WT neurons,

I_{Kv12} was scaled (to 0.5 pA) to reflect the day–night difference in the (mean) CX4-sensitive current amplitudes measured in WT neurons (Fig. 4 D), and the effects of the subtraction of integral multiples of this value (i.e., x = 0.5 pA) on the repetitive firing rates of daytime WT neurons were determined. As shown in the representative recordings from a WT nighttime SCN neuron in Fig. 6, A–C, subtraction of the minimal I_{Kv12} (−x) increased the rate of repetitive firing (Fig. 6 B), and the rate was increased further when the amplitude of I_{Kv12} was increased (−3x) three-fold (Fig. 6 C). In contrast, as illustrated in the representative recordings from a WT daytime SCN neuron in Fig. 6, E–G, dynamic clamp-mediated subtraction of I_{Kv12} (at −x or −3x) had little to no effect on the rate of spontaneous action potential firing. Similar results were obtained in recordings from additional WT nighttime and daytime SCN neurons in which varying amplitudes (−x, −2x, −3x, −4x, and −5x) of I_{Kv12} were subtracted via a dynamic clamp. The mean ± SEM percent changes in the spontaneous repetitive firing rates of WT daytime (open black square; n = 7) and nighttime (closed black square; n = 10) SCN neurons are plotted as a function of the magnitude of I_{Kv12} subtracted in Fig. 6, D and H. The insets below Fig. 6, C and G, show the waveforms of individual action potentials recorded in the representative WT nighttime (C) and daytime (G) SCN neurons, plotted on an expanded timescale. The modeled (−3x) I_{Kv12} waveforms generated in these cells are shown below the voltage records; the zero current levels are indicated by dotted lines. It is of interest to note that I_{Kv12} increases as the membrane potential approaches the threshold for generating an action potential in the nighttime neuron (Fig. 6 C, inset), and the mean modeled I_{Kv12} amplitudes are larger during interspike intervals in nighttime (1.49 ± 0.15 pA; Fig. 6 C, inset) than in daytime (−0.39 ± 0.05 pA; Fig. 6 G, inset) SCN neurons. These observations are consistent with a selective role for I_{Kv12} in regulating the interspike interval and the rate of spontaneous repetitive action potential firing in nighttime SCN neurons.
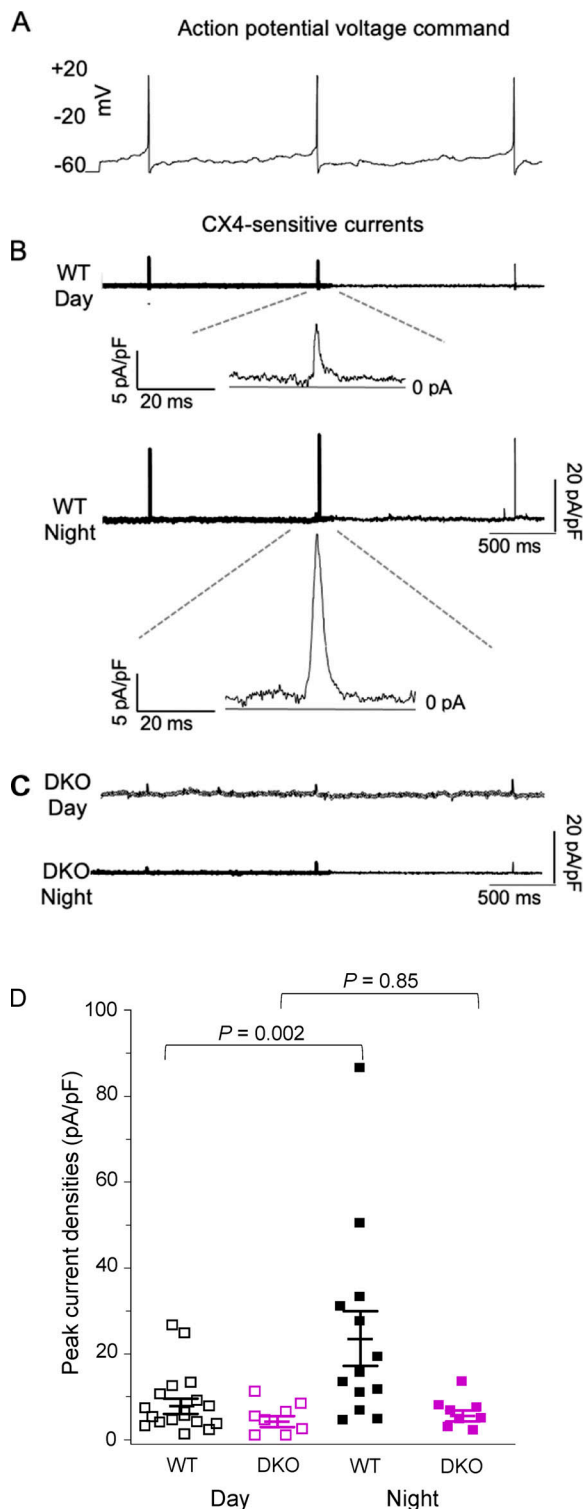
Hermanstyne et al.
Kv12 channels regulate nighttime SCN neuronal firing

Journal of General Physiology   12 of 23
https://doi.org/10.1085/jgp.202213310

A Action potential voltage command

B CX4-sensitive currents

WT Day

WT Night

C DKO Day

DKO Night

D

In contrast with the marked differences in the effects of subtracting I_{Kv12} in WT nighttime and daytime SCN neurons (Fig. 6), dynamic clamp-mediated addition of I_{Kv12} decreased the repetitive firing rates of both nighttime and daytime WT SCN neurons (Fig. 7). The addition of the modeled I_{Kv12} also reduced the rate of repetitive firing in nighttime Kv12.1$^{-/-}$ SCN neurons (Fig. S6, A–C), although the magnitudes of the percent changes in the repetitive firing rates of nighttime Kv12.1$^{-/-}$ SCN neurons were smaller than in nighttime WT SCN neurons (Fig. S6 D).

To determine if the functional effects of dynamic clamp-mediated manipulation of I_{Kv12} observed in WT SCN neurons (Figs. 6 and 7) are specific for I_{Kv12} or, alternatively, are observed when any subthreshold voltage-activated K$^+$ current is added/subtracted, we generated a mathematical model of I_A in SCN neurons. In previous studies, we have shown that shRNA-mediated knockdown of Kv4.1 decreases I_A amplitudes and increases the repetitive firing rates of daytime and nighttime SCN neurons (Hermanstyne et al., 2017). Using acquired voltage-clamp data describing the time- and voltage-dependent properties of I_A in WT SCN neurons (Hermanstyne et al., 2017), we generated a model of I_A gating (Fig. S3). As illustrated in Fig. S7, the modeled I_A waveforms and I_{Kv12} waveforms generated by individual action potentials recorded in a representative WT SCN neuron are distinct.

In experiments similar to those described above for I_{Kv12}, we determined the effects on spontaneous repetitive rates of subtracting/adding I_A, presented in multiples of the minimal I_A, x, determined as described in Materials and methods. Dynamic clamp-mediated subtraction of modeled I_A initially increased the repetitive firing rates of WT nighttime (Fig. 8, A, C, and E) and daytime (Fig. 8, B, D, and F) SCN neurons. With the subtraction of higher amplitude currents, however, repetitive firing rates decreased in WT nighttime (Fig. 8 E) and daytime (Fig. 8 F) SCN neurons. The insets below Fig. 8, C and D, show the waveforms of individual action potentials recorded in the representative WT nighttime (C) and daytime (D) SCN neurons, plotted on an expanded timescale. The modeled (−3x) I_A waveforms generated in these cells are shown below the voltage records: the 0 current levels are indicated by dotted lines. As is evident, there are clear differences in the peak amplitudes of the modeled I_A during the action potentials in WT nighttime (C) and daytime (D) SCN neurons. In addition and in contrast with the results obtained with I_{Kv12} (Fig. 6), I_A is prominent during interspike intervals in WT nighttime (−6.88 ± 0.83 pA; Fig. 8 C, inset) and daytime

Figure 4. CX4-sensitive K$^+$ current densities in SCN neurons are higher at night than during the day. (A) Whole-cell outward K$^+$ currents, evoked by an action potential voltage command recorded from a nighttime WT SCN neuron, were recorded in WT and DKO (Kv12.1$^{-/-}$/Kv12.2$^{-/-}$) SCN neurons before and after local application 20 μM CX4. Subtraction of the currents recorded before/after application of CX4 in each cell provided the CX4-sensitive K$^+$ currents. **(B and C)** Representative CX4-sensitive outward K$^+$ currents, obtained by offline digital subtraction of the currents recorded in the presence of CX4 from the currents recorded (in the same cell) in the control bath solution during the day and at night in WT (B) and DKO (C) SCN neurons, are shown. The CX4-sensitive outward K$^+$ currents recorded in WT daytime and nighttime SCN neurons are also displayed on an expanded time scale in the insets in B. **(D)** Peak CX4-sensitive K$^+$ current densities measured in WT (black squares) and DKO (magenta squares) SCN neurons during the day and at night are plotted. The mean ± SEM CX4-sensitive K$^+$ current density in WT (black squares) SCN neurons is much higher (P = 0.002, one-way ANOVA) at night (n = 13) than during the day (n = 17). In contrast, CX4-sensitive K$^+$ current densities in DKO (magenta squares) SCN neurons are low during the day (n = 8) and at night (n = 8), and there is no day–night difference (P = 0.85, one-way ANOVA) in mean ± SEM CX4-sensitive K$^+$ current densities in DKO (magenta squares) SCN neurons.

Hermanstyne et al.
Kv12 channels regulate nighttime SCN neuronal firing

Journal of General Physiology   13 of 23
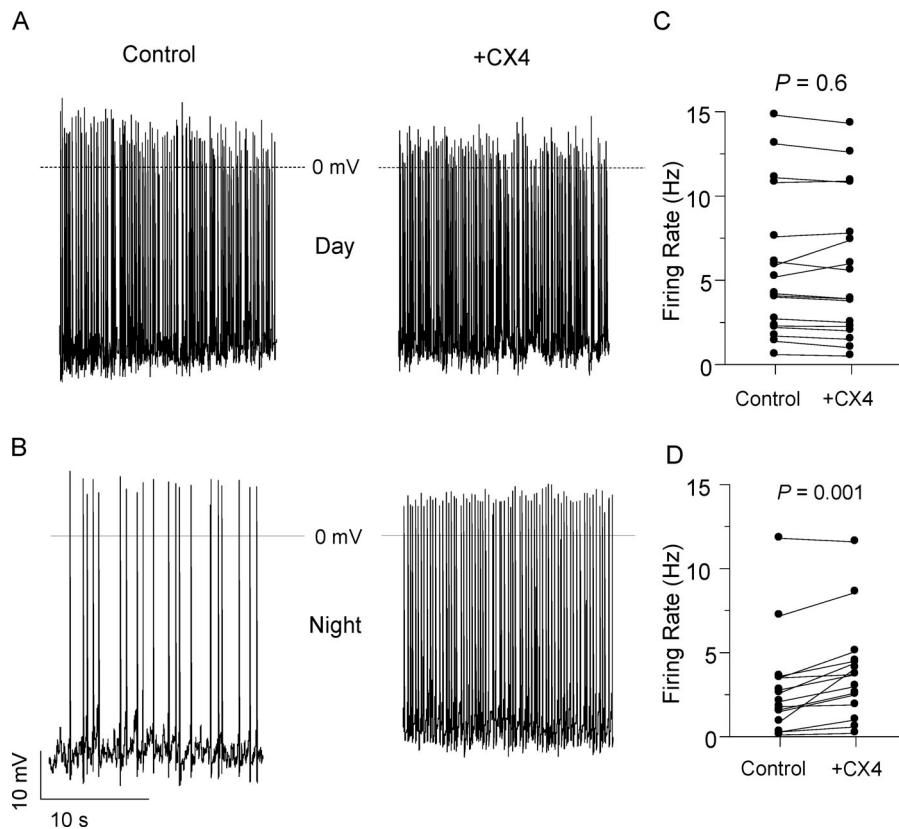https://doi.org/10.1085/jgp.202213310

Figure 5. **Pairwise comparisons of repetitive firing rates in WT SCN neurons in the absence and presence of CX4. (A and B)** Representative daytime (A) and nighttime (B) whole-cell current-clamp recordings obtained from WT SCN neurons before and after application of 20 μM CX4 are shown. **(C and D)** The repetitive firing rates measured in individual daytime (C) and nighttime (D) WT SCN neurons before and after application of 20 μM CX4 are plotted. In the vast majority (15 of 17; ~90%) of WT SCN neurons, daytime repetitive firing rates were not affected (P = 0.6, repeated measures t test) by the application of 20 μM CX4 (C). In contrast, nighttime repetitive firing rates were increased (P = 0.001, repeated-measures Student's t test) in most (11 of 15; ~70%) WT SCN neurons upon application of 20 μM CX4 (D). Approximately 30% (4 of 15) of nighttime WT SCN neurons, however, were not measurably affected by 20 μM CX4.

(−7.03 ± 0.34 pA; Fig. 8 D, inset) SCN neurons, an observation consistent with the physiological role of I_A in driving the repetitive firing rates of SCN neurons during the day and at night (Hermanstyne et al., 2017). The addition of modeled I_A also decreased the spontaneous repetitive firing rates of WT nighttime (Fig. 9, A, C, and E) and daytime (Fig. 9, B, D, and F) SCN neurons similarly.

Additional experiments were completed to examine the effects of subtracting modeled I_{Kv12} versus modeled I_A in the same daytime cell. As in the experiments presented in Fig. 8, the subtraction of I_A initially increased repetitive firing rates (Fig. S8, A and B), and at higher current amplitudes, firing became unreliable (Fig. S8 C). In contrast, subtraction of I_{Kv12} in the same cell had very little effect on repetitive firing rates (Fig. S8, D–F), with results similar to those presented in Fig. 6. The functional effects of subtracting modeled I_A versus modeled I_{Kv12} on the repetitive firing rates of SCN neurons, therefore, are distinct.

Kcnh8 and Kcnh3 transcript expression in the SCN do not display 24-h rhythms
The results of the action potential- (voltage-) clamp experiments (Fig. 4) demonstrate that amplitudes/densities of the CX4-sensitive, Kv12-encoded K⁺ currents in SCN neurons are higher at night than during the day, suggesting that the functional expression of the underlying K⁺ channels is regulated by the molecular clock. To determine if this regulation reflects day–night differences in the expression levels of the Kcnh transcripts encoding the Kv12.1 (Kcnh8) and Kv12.2 (Kcnh3) α

subunits, quantitative real-time PCR (qRT-PCR) analysis was performed on RNA samples extracted from WT SCN (n = 7–8) every 4 h over two consecutive days. The expression levels of the transcripts encoding the clock genes, Per2 and Bmal (Reppert and Weaver, 2001; Hastings et al., 2018, 2019; Michel and Meijer, 2020), and of Hprt (control gene) in every sample were also determined. Expression of the Per2, Bmal, Kcnh8, and Kcnh3 transcripts was normalized to Hprt in the same sample and evaluated for rhythmicity using JTK cycle analysis (Hughes et al., 2010) with the period set to 24 h. As expected, these analyses revealed that Per2 and Bmal display ~24 h anti-phase rhythms (Fig. S9) in expression (Reppert and Weaver, 2001; Hastings et al., 2018, 2019; Michel and Meijer, 2020). In contrast, the mRNA expression levels of Kcnh8 and Kcnh3 do not (P > 0.05, JTK cycle Bonferroni-adjusted) display 24-h rhythms (Fig. S8), indicating that oscillations in the expression of the Kcnh8 and/or Kcnh3 transcripts do not underlie the observed day–night differences in the functional expression of Kv12-encoded currents (see Discussion).

Loss of Kv12 channels does not eliminate rhythms in (wheel-running) locomotor activity
Representative recordings of wheel-running activity in WT, Kv12.1⁻/⁻, and Kv12.2⁻/⁻ mice are presented in Fig. 10 A. In these experiments, all mice were entrained to a standard 12:12 h LD cycle for 10 d, followed by at least 20 d in DD (Fig. 10 A). Circadian periods were measured in each animal after 20 d in DD (Fig. 10 C). The mean ± SEM circadian periods determined in adult WT (23.6 ± 0.1 h; n = 9), Kv12.1⁻/⁻ (23.5 ± 0.1 h;

Hermanstyne et al.
Kv12 channels regulate nighttime SCN neuronal firing

Journal of General Physiology 14 of 23
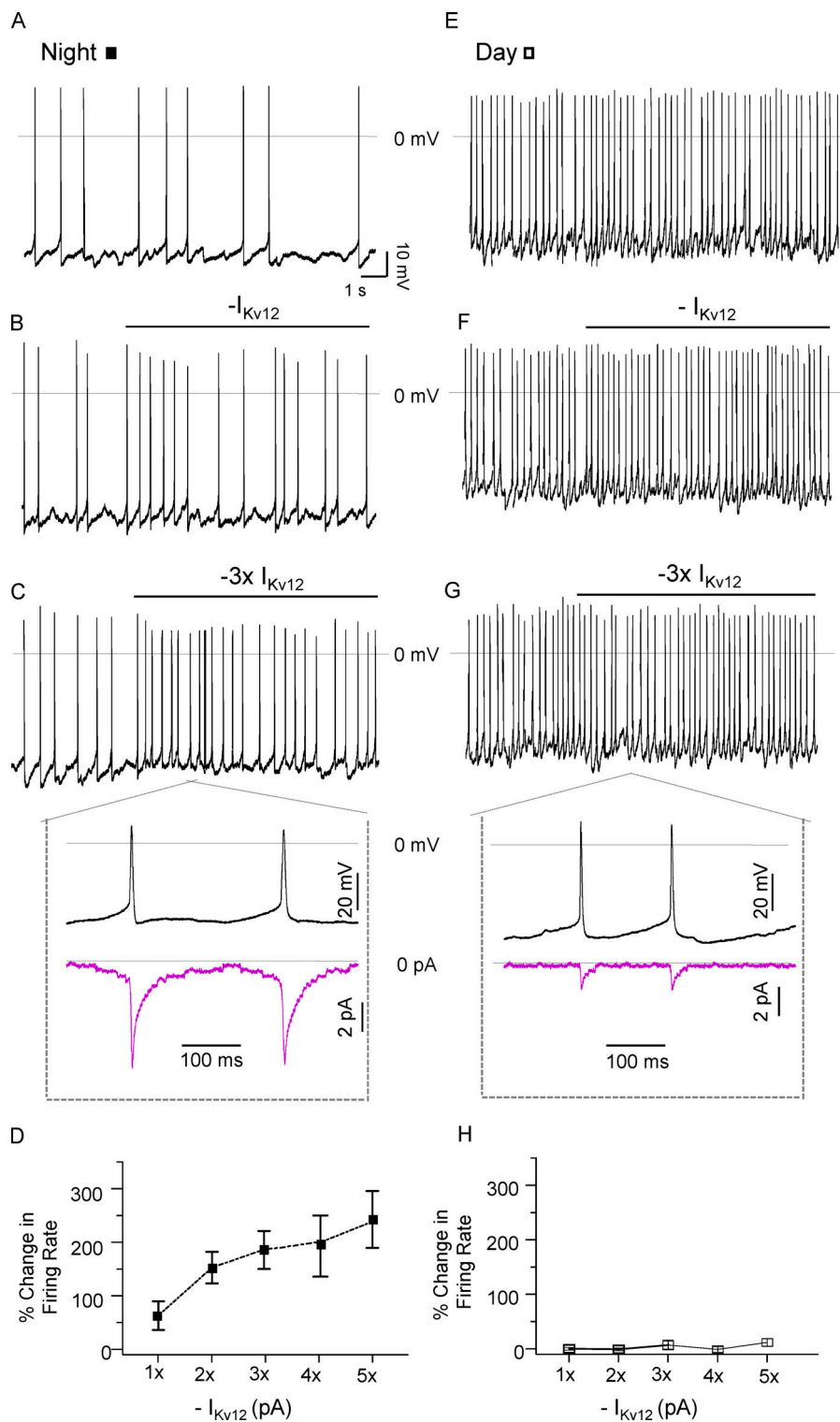https://doi.org/10.1085/jgp.202213310

Figure 6. Dynamic clamp-mediated subtraction of I_{Kv12} increases the repetitive firing rates of nighttime WT SCN neurons. (A–C, and E–G) Representative whole-cell current-clamp recordings from a WT nighttime (A–C) and a WT daytime (E–G) SCN neuron at baseline (A and E) and with different magnitudes of modeled I_{Kv12} subtracted (B, C, F, and G) via dynamic clamp are shown. In the insets below C and G, the waveforms of individual action potentials (black) recorded in the representative WT nighttime (C) and daytime (G) SCN neurons are displayed and plotted on an expanded timescale. Below these voltage records, the modeled (−3x) I_{Kv12} waveforms (purple) are shown; the zero current levels are indicated by the dotted lines. As is evident, the effect of subtracting increasing I_{Kv12} is greater in the nighttime (B and C), than in the daytime (F and G), WT SCN neuron. Similar results were obtained in current-clamp recordings from additional WT nighttime and daytime SCN neurons in which varying amplitudes (−x, −2x, −3x, −4x, and −5x) of the minimal modeled I_{Kv12} (0.5 pA) were subtracted via dynamic clamp. **(D and H)** The mean ± SEM percent changes in the spontaneous repetitive firing rates of WT daytime (empty square; $n = 10$) and nighttime (filled square; $n = 7$) SCN neurons are plotted as a function of the magnitude of modeled I_{Kv12} subtracted.

$n = 15$), Kv12.2$^{-/-}$ (23.6 ± 0.1 h; $n = 14$), and DKO (23.4 ± 0.1 h; $n = 12$, data not shown) animals are indistinguishable (Fig. 10 C). Additional experiments conducted on WT mice 2 wk following bilateral injections of the Kv12.1-targeted, Kv12.2-targeted, or NT-shRNA-expressing AAV8 into the SCN revealed that the acute in vivo knockdown of Kv12.1 or Kv12.2 in the adult SCN also did not disrupt rhythmic wheel-running activity (Fig. 10, B and D).

Discussion

The results of the experiments detailed here demonstrate that the targeted deletion of Kv12.1 or Kv12.2 or the shRNA-mediated knockdown of Kv12.1 or Kv12.2 selectively increased the repetitive firing rates of SCN neurons at night and eliminated the day–night difference in mean repetitive firing rates that is characteristic of WT SCN neurons (Brown and Piggins, 2007; Allen et al., 2017; Belle and Allen, 2018; Harvey
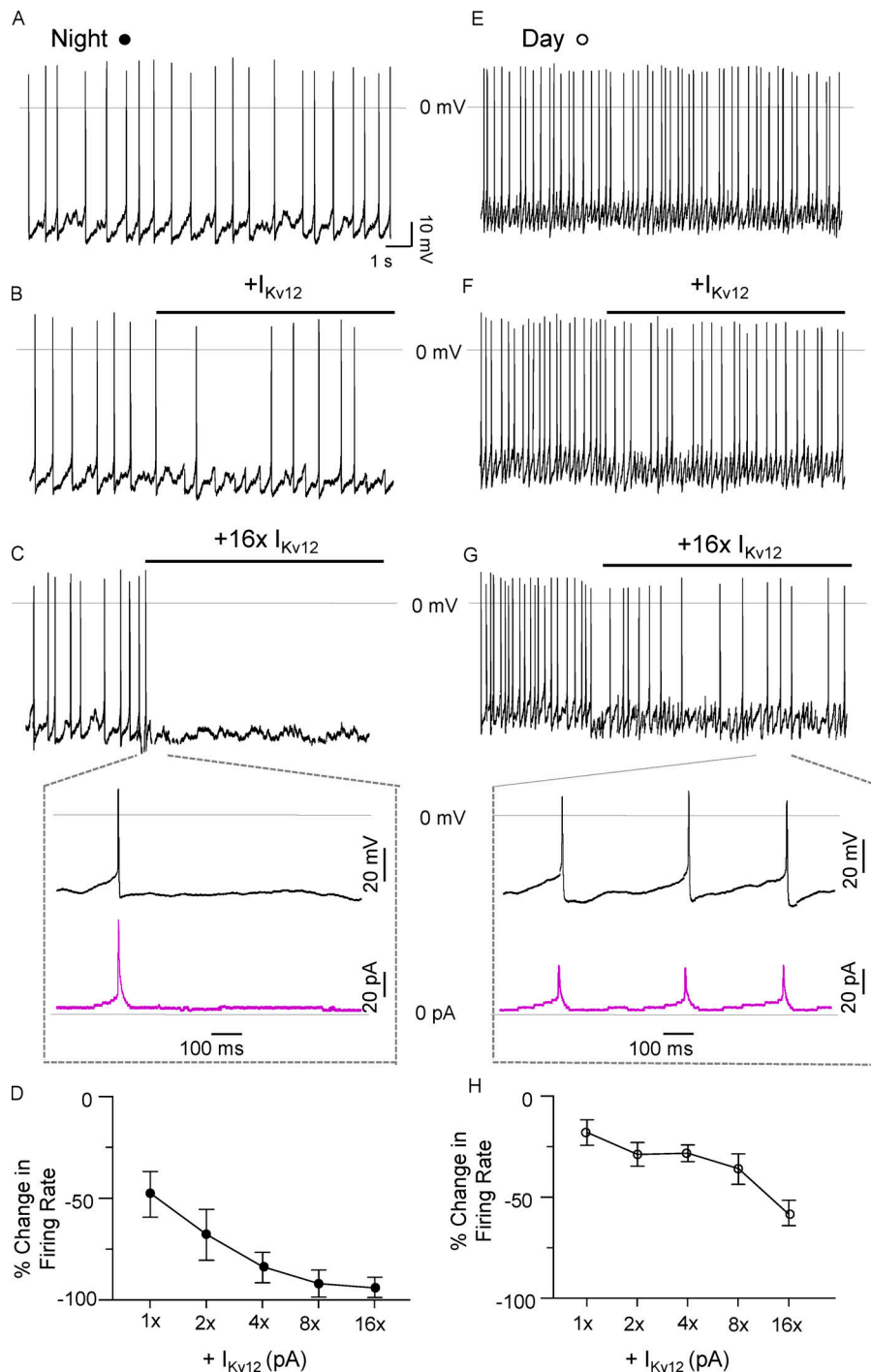
Figure 7. **Dynamic clamp-mediated addition of modeled Kv12-encoded (I_{Kv12}) currents in WT SCN neurons. (A–C, and E–G)** Representative whole-cell current-clamp recordings from a WT nighttime (A–C) and a WT daytime (E–G) SCN neuron at baseline (A and E) and with different magnitudes of modeled I_{Kv12} added (B, C, F, and G) via dynamic clamp are shown. In the insets below C and G, the waveforms of individual action potentials (black) recorded in the representative WT nighttime (C) and daytime (G) SCN neurons are displayed and plotted on an expanded timescale. Below these voltage records, the modeled (+16x) I_{Kv12} waveforms (purple) are shown; the dotted lines indicate the zero current levels. As is evident, increasing I_{Kv12} reduced the rate of repetitive firing in both the WT nighttime (B and C) and the WT daytime (F and G) SCN neuron, although the impact is greater on nighttime (B and C) than on daytime (F and G) firing. Similar results were obtained in recordings from additional WT nighttime and daytime SCN neurons in which varying amplitudes (+x, +2x, +4x, +8x, and +16x) of the minimal modeled I_{Kv12} (2 pA) were added during current-clamp recordings. **(D and H)** The mean ± SEM percent changes in the spontaneous repetitive firing rates of WT daytime (empty circles, $n = 7$) and nighttime (filled circles, $n = 10$) SCN neurons are plotted as a function of the magnitude of modeled I_{Kv12} added.

et al., 2020). Direct application of the Kv12 channel blocker CX4 (Zhang et al., 2010) increased repetitive firing rates at night, but not during the day, and the amplitudes of CX4-sensitive currents in WT SCN neurons were found to be higher at night than during the day. Additional experiments revealed that dynamic clamp-mediated subtraction of modeled I_{Kv12} selectively increased the repetitive firing rates of nighttime, and not daytime, SCN neurons. Despite the loss of day–night oscillations in mean repetitive firing rates, mice lacking Kv12.1 or/and Kv12.2 currents display daily rhythms in locomotor (wheel-running) activity.

Kv12 channels selectively regulate the nighttime repetitive firing properties of SCN neurons

The targeted deletion of either *Kcnh3* (Kv12.2) or *Kcnh8* (Kv12.1) selectively increased the rate of spontaneous action potential firing of SCN neurons at night; the daytime repetitive firing rates of SCN neurons lacking Kv12.1 or Kv12.2 are indistinguishable from WT cells. The higher repetitive firing rates in nighttime Kv12.1$^{-/-}$ and Kv12.2$^{-/-}$ compared with WT, SCN neurons are accompanied by higher input resistances and depolarized membrane potentials. The selective effects on nighttime firing rates and membrane properties were also observed
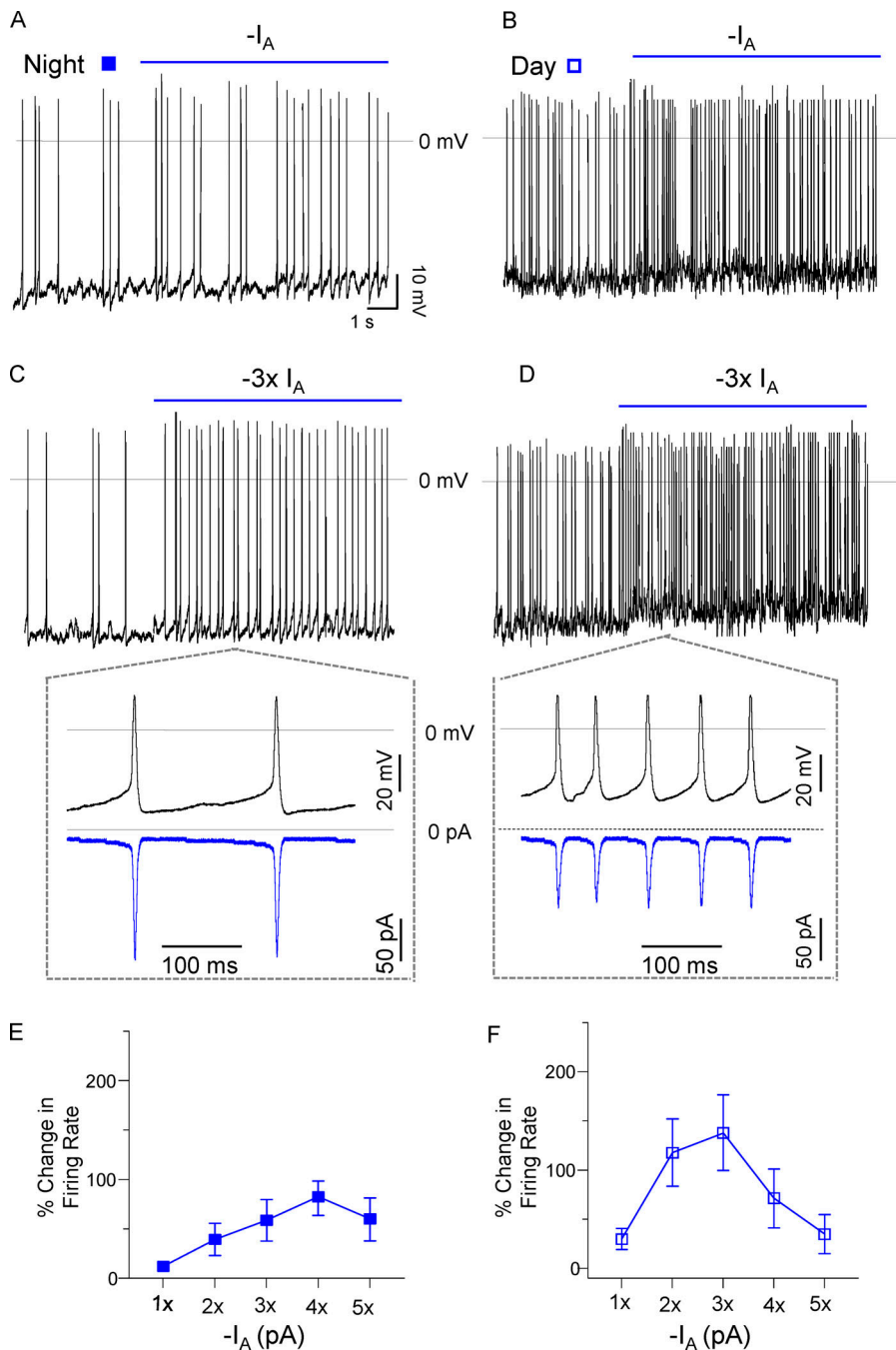
Hermanstyne et al.
Kv12 channels regulate nighttime SCN neuronal firing

Journal of General Physiology
https://doi.org/10.1085/jgp.202213310

16 of 23

Figure 8. **Dynamic clamp-mediated subtraction of modeled I_A in WT SCN neurons. (A–D)** Representative whole-cell current-clamp recordings from WT nighttime (A and C) and daytime (B and D) SCN neurons with different magnitudes of modeled I_A subtracted are shown. In the insets below C and D, the waveforms of individual action potentials (black), recorded in the representative WT nighttime (C) and daytime (D) SCN neurons, are plotted on an expanded timescale. The modeled (−3x) I_{Kv12} waveforms (blue) generated in these cells are shown; the zero current levels are indicated by the dotted lines. As is evident, the rates of repetitive firing of the representative nighttime (A and C) and daytime (B and D) SCN neurons are increased with the subtraction of modeled I_A. Similar results were obtained in recordings from additional nighttime and daytime WT SCN in which varying amplitudes of the minimal modeled I_A (20 pA) were subtracted (−x, −2x, −3x, −4x, and −5x) during current-clamp recordings. **(E and F)** The mean ± SEM percent changes in the spontaneous repetitive firing rates of WT SCN neurons in response to subtracting (open and closed squares; n = 16) modeled I_A are plotted as a function of the magnitude of the modeled I_A subtracted.

in DKO SCN neurons lacking both Kv12.1 and Kv12.2 (Table 1). Acute, in vivo Kv12.1-targeted or Kv12.2-targeted shRNA-mediated knockdown of Kv12.1 or Kv12.2 in adult SCN neurons also selectively increased nighttime repetitive firing rates (Table 2). In addition to demonstrating a critical physiological role for Kv12-encoded K^{+} channels in regulating the nighttime firing and membrane properties of mature SCN neurons, these results also suggest that the firing properties of Kv12.1[−/−], Kv12.2[−/−], and Kv12.1[−/−]/Kv12.2[−/−] SCN neurons do not reflect effects secondary to the loss of Kv12.1/Kv12.2 channels throughout development. Mimicking the effects of knockout/knockdown of Kv12.1/Kv12.2, dynamic clamp-mediated subtraction of I_{Kv12} selectively increased the repetitive firing rates

of WT nighttime SCN neurons. These results contrast with the effects of manipulating another subthreshold K^{+} current, I_A: dynamic clamp-mediated subtraction of I_A increased spontaneous repetitive firing rates in WT nighttime and daytime SCN neurons.

Application of 20-μM CX4 also selectively increased the spontaneous repetitive firing rates of nighttime WT SCN neurons, and voltage-clamp experiments revealed that CX4-sensitive outward K^{+} currents are higher in nighttime than in daytime WT SCN neurons. In the original study characterizing CX4 (Zhang et al., 2010), however, it was reported that CX4 is a selective blocker of heterologously expressed Kv12.2-encoded K^{+} currents and that expressed Kv12.1-encoded K^{+} currents were
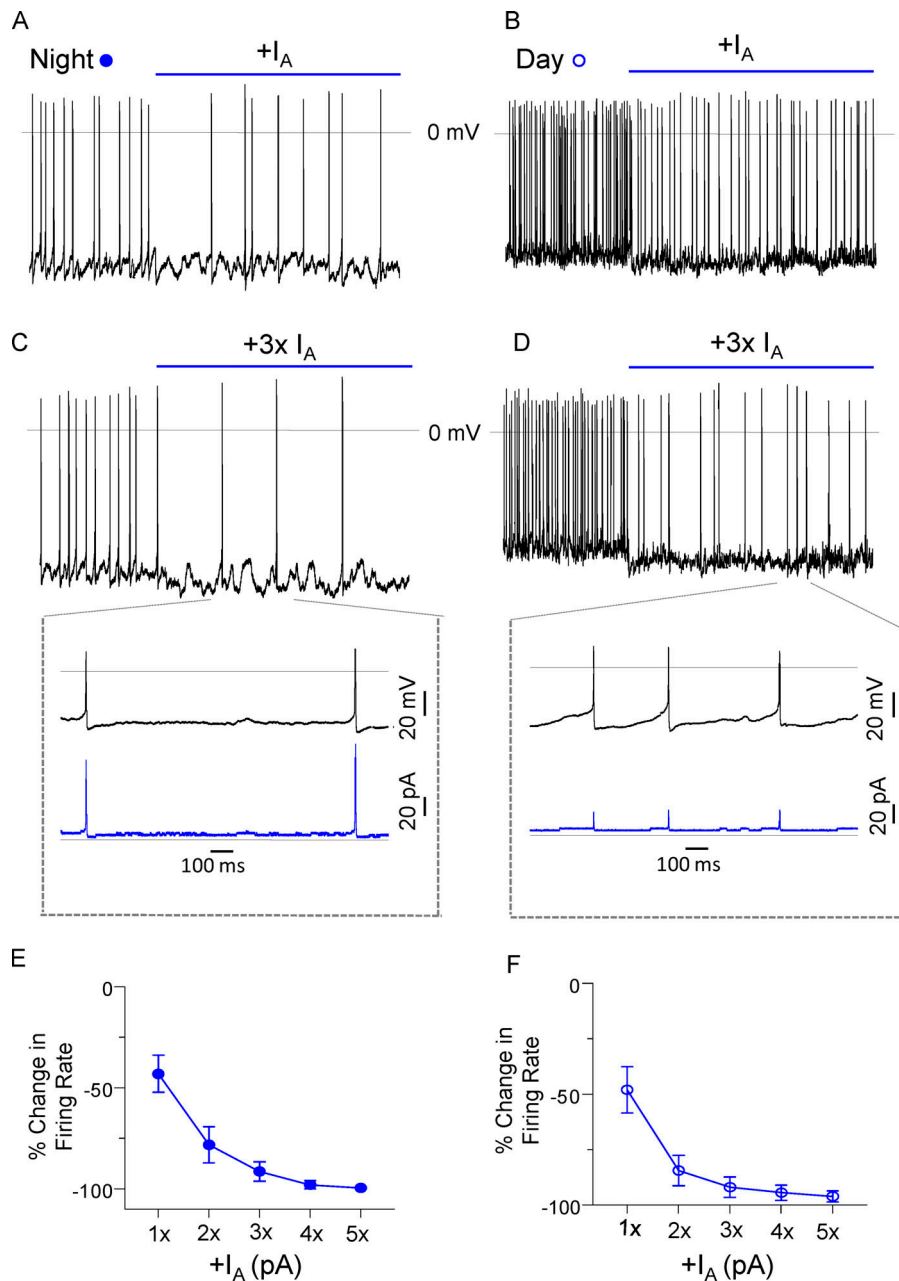
Figure 9. **Dynamic clamp-mediated addition of modeled I_A in WT SCN neurons. (A–D)** Representative whole-cell current-clamp recordings from WT nighttime (A and C) and daytime (B and D) SCN neurons with different magnitudes of modeled I_A added are shown. In the insets below C and D, the waveforms of individual action potentials (black), recorded in the representative WT nighttime (C) and daytime (D) SCN neurons, are plotted on an expanded timescale. The modeled (+3x) I_{Kv12} waveforms (blue) generated in these cells are shown; the zero current levels are indicated by the dotted lines. The rates of repetitive firing of both the representative nighttime (A and C) and the representative daytime (B and D) SCN neurons are decreased with the addition of modeled I_A. Recordings from additional nighttime and daytime WT SCN neurons in which varying amplitudes (x, 2x, 3x, 4x, 5x) of the minimal modeled I_A (20 pA) were added also revealed a decrease in repetitive firing rates. **(E–H)** The mean ± SEM percent changes in the spontaneous repetitive firing rates of WT SCN neurons in response to adding (open and closed circles; $n = 14$) modeled I_A are plotted as a function of the magnitude of the modeled I_A added.

unaffected by CX4. The finding here that application of 20 μM CX4 markedly increases the repetitive firing rates of nighttime SCN neurons, similar to the knockout/knockdown of either Kv12.1 or Kv12.2, suggests that CX4 may also affect Kv12.1-encoded K⁺ channels in native (neuronal) cells. Alternatively, these results may suggest that Kv12.1 and Kv12.2 form heteromeric channels in SCN neurons. The presence of the residual CX-sensitive outward K⁺ currents in DKO SCN neurons (Fig. 4) reveals another caveat with the interpretation of these pharmacological experiments, i.e., there is a component(s) of the CX4-sensitive outward K⁺ currents that reflects the effects of CX4 on non-Kv12-encoded K⁺ channels. Additional experiments will be needed to identify the molecular determinant(s) of the residual, non-Kv12-encoded component of the CX4-insensitive currents in SCN neurons.

Relationship to previous studies

Several previous studies have demonstrated selective roles for other (i.e., non-Kv12-encoded) types of K⁺ channels in regulating the daytime and/or nighttime repetitive firing rates of SCN neurons. Acute in vivo shRNA-mediated knockdown of *Kcnd1*, which encodes the Kv4.1 α subunit and contributes to the generation of I_A, in adult SCN neurons affects daytime and nighttime I_A densities and spontaneous firing rates (Hermanstyne et al., 2017). The densities of I_A were lower in Kv4.1-targeted shRNA-expressing compared with WT, SCN neurons during the day and at night (Hermanstyne et al., 2017). Knockdown of Kv4.1 also increased repetitive firing rates during the day and at night (Hermanstyne et al., 2017). In contrast with the effects of the knockdown or deletion of Kv12 channels, the loss of Kv4.1-encoded I_A channels did not eliminate day–night oscillations in the
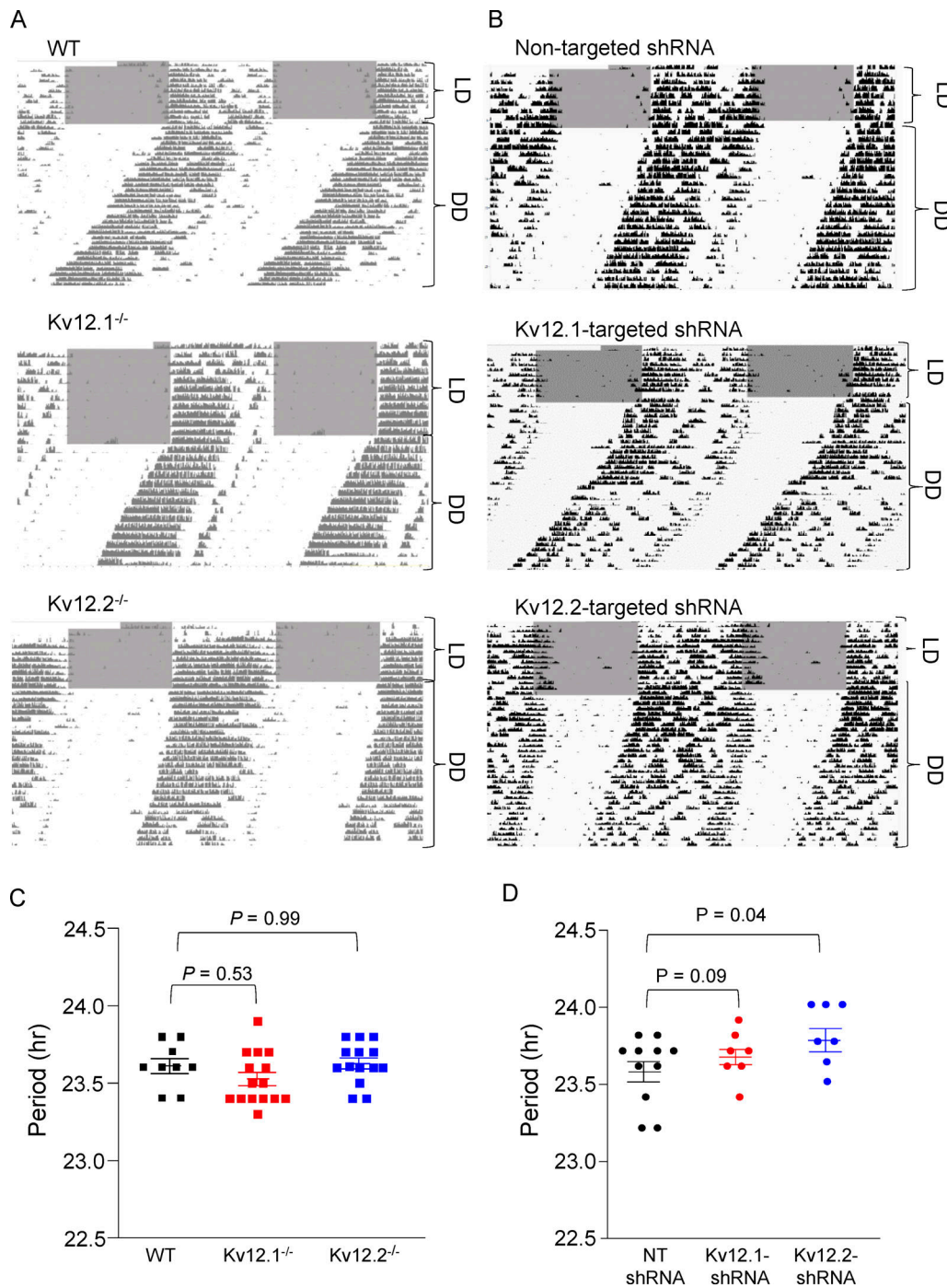
Figure 10. **Rhythmic wheel-running activity is maintained in Kv12.1$^{-/-}$ and Kv12.2$^{-/-}$ mice and with acute in vivo shRNA-mediated knockdown of Kv12.1 or Kv12.2 in adult animals. (A and B)** Representative recordings of wheel-running activity of WT (top), Kv12.1$^{-/-}$ (middle), and Kv12.2$^{-/-}$ (bottom) mice (A) and WT mice that received bilateral SCN injections of the non-targeted (top), Kv12.1-targeted (middle), or Kv12.2-targeted (bottom) shRNA-expressing AAV8 (B). Continuous recordings were obtained for ~10 d in 12:12 h LD (indicated by the grey and white backgrounds, respectively) conditions, followed by at least 20 d in DD (constant darkness, indicated by the white background). The circadian periods, measured in each WT (black squares), Kv12.1$^{-/-}$ (red squares), and Kv12.2$^{-/-}$ (blue squares) mouse and in each animal expressing the NT (black circles), Kv12.1-targeted (red circles) and Kv12.2-targeted (blue circles) shRNA in DD, are plotted; P values (one-way ANOVA are indicated). **(C)** The mean ± SEM circadian periods of locomotor activity determined in WT (black squares; n = 9), Kv12.1$^{-/-}$ (red squares; n = 15) and Kv12.2$^{-/-}$ (blue squares; n = 14) are similar. **(D)** The mean ± SEM circadian periods (D) of locomotor activity measured in animals expressing the Kv12.1-targeted shRNA (red circles; n = 7), the Kv12.2-targeted shRNA (blue circles; n = 7) and the NT shRNA (black circles; n = 11) are also similar.

Hermanstyne et al.
Kv12 channels regulate nighttime SCN neuronal firing

Journal of General Physiology   19 of 23
https://doi.org/10.1085/jgp.202213310

repetitive firing rates of SCN neurons (Hermanstyne et al., 2017). Also in contrast with the results here, in vivo knockdown of Kv4.1-encoded I_A channels advanced the time of daily activity onset by ∼1.8 h and shortened the periods of wheel-running activity in constant darkness by ∼0.5 h (Hermanstyne et al., 2017).

In contrast with the effects of manipulating I_A (Granados-Fuentes et al., 2012, 2015; Hermanstyne et al., 2017), targeted deletion of *Kcnma1*, which encodes the pore-forming α subunit of large conductance voltage- and Ca^{2+}-dependent K^+ (BK) channels, results in increased repetitive firing rates selectively in nighttime SCN neurons (Meredith et al., 2006), markedly reducing the day–night oscillation in mean repetitive firing rates, characteristic of WT SCN neurons (Brown and Piggins, 2007; Allen et al., 2017; Belle and Allen, 2018; Harvey et al., 2020). The circadian periods of locomotor activity and clock gene expression in *Kcnma1*$^{−/−}$ animals, however, were indistinguishable from WT animals, although the circadian amplitudes of wheel-running activity and other behavioral outputs were reduced in *Kcnma1*$^{−/−}$, compared with WT, mice during the day and at night (Meredith et al., 2006). Opposite cellular effects were seen with overexpression of *Kcnma1* in the SCN, i.e., the repetitive firing rates were reduced in the daytime but not in the nighttime SCN neurons (Montgomery et al., 2013). The overexpression of *Kcnma1* and the reduction in daytime repetitive firing rates, however, were not accompanied by changes in the periods or the amplitudes of circadian behaviors (Montgomery et al., 2013).

Previous studies have also demonstrated marked day–night differences in fast delayed rectifier (FDR) K^+ current densities and in the expression of the *Kcnc1* and *Kcnc2* transcripts, which encode the Kv3.1b and Kv3.2 α subunits and generate FDR K^+ currents, in SCN neurons (Itri et al., 2005). In addition, it was reported that exposure to the K^+ channel blocker, 4-aminopyridine (4-AP) at a concentration of 0.5 mM, selectively reduces daytime repetitive firing rates and eliminates daily rhythms in the firing rates of SCN neurons (Itri et al., 2005). Similar effects on daytime firing rates were seen in SCN neurons from (*Kcnc1*$^{−/−}$/*Kcnc2*$^{−/−}$) animals lacking both Kv3.1b and Kv3.2 (Kudo et al., 2011), consistent with the suggestion that 0.5 mM 4-AP selectively affects FDR K^+ currents in SCN neurons (Itri et al., 2005). Despite the elimination of day–night oscillations in repetitive firing rates, daily rhythms in *Per2* expression were intact in *Kcnc1*$^{−/−}$/*Kcnc2*$^{−/−}$ animals (Kudo et al., 2011).

Molecular determinants of day–night differences in Kv12-encoded K^+ current densities in the SCN
Consistent with the selective effects of the deletion or the acute knockdown of Kv12 subunits, action potential- (voltage-) clamp experiments revealed that the mean density of the CX4-sensitive (Kv12-encoded) K^+ currents in WT SCN neurons is much higher at night than during the day. The quantitative RT-PCR analysis completed, however, indicates that the day–night difference in Kv12-encoded K^+ current densities does not result from circadian regulation of the *Kcnh3*/*Kcnh8* transcripts encoding the Kv12.1/Kv12.2 α subunits. Although it is certainly possible that Kv12.1/Kv12.2 protein expression in the SCN is rhythmic despite

no day–night differences in *Kcnh3*/*Kcnh8* transcript expression, exploring this possibility must await the availability of validated anti-Kv12.1 and anti-Kv12.2 antibodies. It is also possible that accessory subunits play a critical role in regulating day–night differences in Kv12-encoded K^+ currents densities, as has been demonstrated for the accessory β2 subunit of *Kcnma1*-encoded BK currents (Whitt et al., 2016).

A rather large number of intracellular and transmembrane accessory subunits of Kv channels have been identified (Paul et al., 2016), and members of at least one subfamily, the *Kcne* subfamily, have been shown to regulate the expression and properties of Kv12.2-encoded K^+ channels (Clancy et al., 2009). Reducing *Kcne1* or *Kcne3* expression in *Xenopus* oocytes, for example, increased the amplitudes of heterologously expressed Kv12.2 currents, whereas overexpression of *Kcne1* or *Kcne3* reduced Kv12.2 current amplitudes (Clancy et al., 2009). Additional experiments revealed that manipulating *Kcne1* or *Kcne3* affected the surface expression of Kv12.2, whereas the total Kv12.2 protein was not affected (Clancy et al., 2009). Although *Kcne1* and *Kcne3*, as well as other *Kcne* subfamily members, are expressed in the SCN (http://circadb.hogeneschlab.org), it is not clear whether any of these transcripts and/or the proteins encoded by these transcripts display daily rhythms in expression. It will be important to explore this possibility directly, as well as to determine the functional consequences of manipulating *Kcne1* or *Kcne3* expression on the repetitive firing properties of SCN neurons.

Posttranslational modifications of the Kv12.1 and/or Kv12.2 α subunits or of accessory subunits of Kv12-encoded channels could also play a role in modulating Kv12 current densities in SCN neurons by influencing cell-surface channel expression directly or by modifying the conductance and/or the open probability of single Kv12 channels. In this context, it is of interest to note that in vivo constitutive activation of the two isoforms of the serine/threonine kinase glycogen synthase kinase 3, GSK3, previously shown to display rhythms in expression and phosphorylation of components of the molecular clock (Iwahana et al., 2004; Iitaka et al., 2005), altered the repetitive firing rates of SCN neurons and disrupted rhythmic locomotor activity (Paul et al., 2012). Subsequent work revealed that GSK3 regulates the amplitude of the persistent component of the Na^+ current, I_{NaP} (Jackson et al., 2004), in SCN neurons, and that GSK3 inhibition selectively reduced the spontaneous repetitive firing rates of SCN neurons during the day (Paul et al., 2016). It will be of interest to determine if GSK3, or downstream targets of GSK3, plays a role in regulating day–night differences in Kv12-encoded K^+ current densities in the SCN.

Physiological implications
The direct link between the spontaneous firing of action potentials and the output of the SCN was established with the in vivo demonstration that continuous infusion of the voltage-gated Na^+ channel toxin, TTX, into the SCN of unanesthetized and unrestrained animals (rats) disrupted the circadian rhythm of drinking (Schwartz et al., 1987). Additional in vivo experiments revealed a negative correlation between the repetitive firing rates of SCN neurons and wheel-running activity,

Hermanstyne et al.
Kv12 channels regulate nighttime SCN neuronal firing

Journal of General Physiology   20 of 23
https://doi.org/10.1085/jgp.202213310

i.e., wheel-running activity was high at night when repetitive firing rates were low and, conversely, wheel-running activity was low during the day when repetitive firing rates were high (Earnest et al., 1991). In addition, the acute silencing of SCN neurons during the day (by application of TTX) triggered wheel running, an observation interpreted as demonstrating that repetitive firing rates directly determine the temporal profile of behavioral activity (Earnest et al., 1991). In vitro experiments on SCN explants also showed that the application of TTX eliminated firing and circadian rhythms in vasopressin release (Houben et al., 2014).

Given these combined observations, the finding here that the loss of day–night differences in the repetitive firing rates of SCN neurons with the loss/knockdown of Kv12.1/Kv12.2 did not affect the period of wheel-running activity seems surprising. As noted above, however, previous studies revealed that manipulating *Kcnc*-encoded FDR (Itri et al., 2005; Kudo et al., 2011) or *Kcnma1*-encoded BK (Meredith et al., 2006; Montgomery et al., 2013) K⁺ currents reduced/eliminated day–night differences in repetitive firing rates in the SCN, while having little or no effect on rhythmic wheel-running activity (Itri et al., 2005; Meredith et al., 2006; Kudo et al., 2011; Montgomery et al., 2013). One interpretation of the marked difference in the functional consequences of applying TTX versus changing individual K⁺ conductances is that the cellular effects are very different. Manipulating individual K⁺ currents, for example, may alter the daytime and/or nighttime repetitive firing rates of SCN neurons, but, unlike TTX, does not eliminate repetitive firing altogether. In addition, whereas the application of TTX silences all SCN neurons, the impact of manipulating individual K⁺ currents might be highly variable across cells depending on the repertoire and densities of the K⁺ and non-K⁺ channels contributing to shaping individual action potentials and repetitive firing patterns in different cell types (Pennartz et al., 1998; Hermanstyne et al., 2016; Patton et al., 2020). Indeed, the experiments here revealed that the densities of the CX4-sensitive K⁺ currents were quite variable among nighttime SCN neurons. In addition, ~30% of nighttime SCN neurons were unaffected by CX4, indicating that the day–night switch in the repetitive firing properties of this subpopulation(s) of neurons is regulated by distinct (non-Kv12-encoded) K⁺ conductance(s). Given the diversity of cell types in the SCN, distinguished based on morphological features, transmitter phenotypes, synaptic connectivities, and firing properties (Pennartz et al., 1998; Hermanstyne et al., 2016; Allen et al., 2017; Belle and Allen, 2018; Hastings et al., 2018, 2019; Mazuski et al., 2018; Harvey et al., 2020; Michel and Meijer, 2020; Patton et al., 2020), future studies aimed at identifying the critical ionic conductances regulating the intrinsic membrane properties and the day–night oscillations in the repetitive firing rates of SCN should be conducted on identified SCN cell types.

Data availability
The data underlying Figs. 1, 2, 3, 4, 5, 6, 7, 8, 9, and 10; and Tables 1 and 2 are available in the published article and its online supplemental material.

References
Aldrich, R.W., D.P. Corey, and C.F. Stevens. 1983. A reinterpretation of mammalian sodium channel gating based on single channel recording. *Nature*. 306:436–441. https://doi.org/10.1038/306436a0

Allen, C.N., M.N. Nitabach, and C.S. Colwell. 2017. Membrane currents, gene expression, and circadian clocks. *Cold Spring Harb. Perspect. Biol.* 9: a027714. https://doi.org/10.1101/cshperspect.a027714

Aton, S.J., G.D. Block, H. Tei, S. Yamazaki, and E.D. Herzog. 2004. Plasticity of circadian behavior and the suprachiasmatic nucleus following exposure to non-24-hour light cycles. *J. Biol. Rhythms*. 19:198–207. https://doi.org/10.1177/0748730404264156

Becchetti, A., M. De Fusco, O. Crociani, A. Cherubini, R. Restano-Cassulini, M. Lecchi, A. Masi, A. Arcangeli, G. Casari, and E. Wanke. 2002. The functional properties of the human ether-à-go-go-like (HELK2) K⁺ channel. *Eur. J. Neurosci.* 16:415–428. https://doi.org/10.1046/j.1460-9568.2002.02079.x

Belle, M.D.C., and C.N. Allen. 2018. The circadian clock: A tale of genetic-electrical interplay and synaptic integration. *Curr. Opin. Physiol.* 5:75–79. https://doi.org/10.1016/j.cophys.2018.08.002

Bett, G.C., A.D. Kaplan, A. Lis, T.R. Cimato, E.S. Tzanakakis, Q. Zhou, M.J. Morales, and R.L. Rasmusson. 2013. Electronic "expression" of the inward rectifier in cardiocytes derived from human-induced pluripotent stem cells. *Heart Rhythm*. 10:1903–1910. https://doi.org/10.1016/j.hrthm.2013.09.061

Brown, T.M., and H.D. Piggins. 2007. Electrophysiology of the supra-chiasmatic circadian clock. *Prog. Neurobiol.* 82:229–255. https://doi.org/10.1016/j.pneurobio.2007.05.002

Campbell, D.L., R.L. Rasmusson, Y. Qu, and H.C. Strauss. 1993. The calcium-independent transient outward potassium current in isolated ferret right ventricular myocytes. I. Basic characterization and kinetic analysis. *J. Gen. Physiol.* 101:571–601. https://doi.org/10.1085/jgp.101.4.571

Clancy, S.M., B. Chen, F. Bertaso, J. Mamet, and T. Jegla. 2009. KCNE1 and KCNE3 beta-subunits regulate membrane surface expression of Kv12.2 K$^+$ channels in vitro and form a tripartite complex in vivo. *PLoS One.* 4:e6330. https://doi.org/10.1371/journal.pone.0006330

Clerx, M., K.A. Beattie, D.J. Gavaghan, and G.R. Mirams. 2019. Four ways to fit an ion channel model. *Biophys. J.* 117:2420–2437. https://doi.org/10.1016/j.bpj.2019.08.001

Du, C., R.L. Rasmusson, G.C. Bett, B. Franks, H. Zhang, and J.C. Hancox. 2021. Investigation of the effects of the short QT syndrome D172N Kir2.1 mutation on ventricular action potential profile using dynamic clamp. *Front. Pharmacol.* 12:794620. https://doi.org/10.3389/fphar.2021.794620

Du, G., J. Yonekubo, Y. Zeng, M. Osisami, and M.A. Frohman. 2006. Design of expression vectors for RNA interference based on miRNAs and RNA splicing. *FEBS J.* 273:5421–5427. https://doi.org/10.1111/j.1742-4658.2006.05534.x

Earnest, D.J., S.M. Digiorgio, and C.D. Sladek. 1991. Effects of tetrodotoxin on the circadian pacemaker mechanism in suprachiasmatic explants in vitro. *Brain Res. Bull.* 26:677–682. https://doi.org/10.1016/0361-9230(91)90160-L

Engeland, B., A. Neu, J. Ludwig, J. Roeper, and O. Pongs. 1998. Cloning and functional expression of rat ether-à-go-go-like K$^+$ channel genes. *J. Physiol.* 513:647–654. https://doi.org/10.1111/j.1469-7793.1998.647ba.x

Flourakis, M., E. Kula-Eversole, A.L. Hutchison, T.H. Han, K. Aranda, D.L. Moose, K.P. White, A.R. Dinner, B.C. Lear, D. Ren, et al. 2015. A conserved bicycle model for circadian clock control of membrane excitability. *Cell.* 162:836–848. https://doi.org/10.1016/j.cell.2015.07.036

Granados-Fuentes, D., T.O. Hermanstyne, Y. Carrasquillo, J.M. Nerbonne, and E.D. Herzog. 2015. IA channels encoded by Kv1.4 and Kv4.2 regulate circadian period of PER2 expression in the suprachiasmatic nucleus. *J. Biol. Rhythms.* 30:396–407. https://doi.org/10.1177/0748730415593377

Granados-Fuentes, D., A.J. Norris, Y. Carrasquillo, J.M. Nerbonne, and E.D. Herzog. 2012. I_A channels encoded by Kv1.4 and Kv4.2 regulate neuronal firing in the suprachiasmatic nucleus and circadian rhythms in locomotor activity. *J. Neurosci.* 32:10045–10052. https://doi.org/10.1523/JNEUROSCI.0174-12.2012

Harvey, J.R.M., A.E. Plante, and A.L. Meredith. 2020. Ion channels controlling circadian rhythms in suprachiasmatic nucleus excitability. *Physiol. Rev.* 100:1415–1454. https://doi.org/10.1152/physrev.00027.2019

Hastings, M.H., E.S. Maywood, and M. Brancaccio. 2018. Generation of circadian rhythms in the suprachiasmatic nucleus. *Nat. Rev. Neurosci.* 19:453–469. https://doi.org/10.1038/s41583-018-0026-z

Hastings, M.H., E.S. Maywood, and M. Brancaccio. 2019. The mammalian circadian timing system and the suprachiasmatic nucleus as its pacemaker. *Biology.* 8:13. https://doi.org/10.3390/biology8010013

Hattar, S., M. Kumar, A. Park, P. Tong, J. Tung, K.W. Yau, and D.M. Berson. 2006. Central projections of melanopsin-expressing retinal ganglion cells in the mouse. *J. Comp. Neurol.* 497:326–349. https://doi.org/10.1002/cne.20970

Hermanstyne, T.O., D. Granados-Fuentes, R.L. Mellor, E.D. Herzog, and J.M. Nerbonne. 2017. Acute knockdown of Kv4.1 regulates repetitive firing rates and clock gene expression in the suprachiasmatic nucleus and daily rhythms in locomotor behavior. *eNeuro.* 4:ENEURO.0377-16.2017. https://doi.org/10.1523/ENEURO.0377-16.2017

Hermanstyne, T.O., C.L. Simms, Y. Carrasquillo, E.D. Herzog, and J.M. Nerbonne. 2016. Distinct firing properties of vasoactive intestinal peptide-expressing neurons in the suprachiasmatic nucleus. *J. Biol. Rhythms.* 31:57–67. https://doi.org/10.1177/0748730415619745

Houben, T., C.P. Coomans, and J.H. Meijer. 2014. Regulation of circadian and acute activity levels by the murine suprachiasmatic nuclei. *PLoS One.* 9:e110172. https://doi.org/10.1371/journal.pone.0110172

Hughes, M.E., J.B. Hogenesch, and K. Kornacker. 2010. JTK_CYCLE: An efficient nonparametric algorithm for detecting rhythmic components in genome-scale data sets. *J. Biol. Rhythms.* 25:372–380. https://doi.org/10.1177/0748730410379711

Iitaka, C., K. Miyazaki, T. Akaike, and N. Ishida. 2005. A role for glycogen synthase kinase-3β in the mammalian circadian clock. *J. Biol. Chem.* 280:29397–29402. https://doi.org/10.1074/jbc.M503526200

Inouye, S.T., and H. Kawamura. 1979. Persistence of circadian rhythmicity in a mammalian hypothalamic "island" containing the suprachiasmatic nucleus. *Proc. Natl. Acad. Sci. USA.* 76:5962–5966. https://doi.org/10.1073/pnas.76.11.5962

Itri, J.N., S. Michel, M.J. Vansteensel, J.H. Meijer, and C.S. Colwell. 2005. Fast delayed rectifier potassium current is required for circadian neural activity. *Nat. Neurosci.* 8:650–656. https://doi.org/10.1038/nn1448

Itri, J.N., A.M. Vosko, A. Schroeder, J.M. Dragich, S. Michel, and C.S. Colwell. 2010. Circadian regulation of a-type potassium currents in the suprachiasmatic nucleus. *J. Neurophysiol.* 103:632–640. https://doi.org/10.1152/jn.00670.2009

Iwahana, E., M. Akiyama, K. Miyakawa, A. Uchida, J. Kasahara, K. Fukunaga, T. Hamada, and S. Shibata. 2004. Effect of lithium on the circadian rhythms of locomotor activity and glycogen synthase kinase-3 protein expression in the mouse suprachiasmatic nuclei. *Eur. J. Neurosci.* 19:2281–2287. https://doi.org/10.1111/j.0953-816X.2004.03322.x

Jackson, A.C., G.L. Yao, and B.P. Bean. 2004. Mechanism of spontaneous firing in dorsomedial suprachiasmatic nucleus neurons. *J. Neurosci.* 24:7985–7998. https://doi.org/10.1523/JNEUROSCI.2146-04.2004

Kazmierczak, M., X. Zhang, B. Chen, D.K. Mulkey, Y. Shi, P.G. Wagner, K. Pivaroff-Ward, J.K. Sassic, D.A. Bayliss, and T. Jegla. 2013. External pH modulates EAG superfamily K$^+$ channels through EAG-specific acidic residues in the voltage sensor. *J. Gen. Physiol.* 141:721–735. https://doi.org/10.1085/jgp.201210938

Kemler, R., A. Hierholzer, B. Kanzler, S. Kuppig, K. Hansen, M.M. Taketo, W.N. de Vries, B.B. Knowles, and D. Solter. 2004. Stabilization of β-catenin in the mouse zygote leads to premature epithelial-mesenchymal transition in the epiblast. *Development.* 131:5817–5824. https://doi.org/10.1242/dev.01458

Kent, J., and A.L. Meredith. 2008. BK channels regulate spontaneous action potential rhythmicity in the suprachiasmatic nucleus. *PLoS One.* 3:e3884. https://doi.org/10.1371/journal.pone.0003884

Kudo, T., D.H. Loh, D. Kuljis, C. Constance, and C.S. Colwell. 2011. Fast delayed rectifier potassium current: Critical for input and output of the circadian system. *J. Neurosci.* 31:2746–2755. https://doi.org/10.1523/JNEUROSCI.5792-10.2011

Kuhlman, S.J., and D.G. McMahon. 2006. Encoding the ins and outs of circadian pacemaking. *J. Biol. Rhythms.* 21:470–481. https://doi.org/10.1177/0748730406294316

Kumar Jha, P., E. Challet, and A. Kalsbeek. 2015. Circadian rhythms in glucose and lipid metabolism in nocturnal and diurnal mammals. *Mol. Cell. Endocrinol.* 418:74–88. https://doi.org/10.1016/j.mce.2015.01.024

Li, X., A. Anishkin, H. Liu, D.B. van Rossum, S.V. Chintapalli, J.K. Sassic, D. Gallegos, K. Pivaroff-Ward, and T. Jegla. 2015. Bimodal regulation of an Elk subfamily K$^+$ channel by phosphatidylinositol 4,5-bisphosphate. *J. Gen. Physiol.* 146:357–374. https://doi.org/10.1085/jgp.201511491

Marionneau, C., S. Brunet, T.P. Flagg, T.K. Pilgram, S. Demolombe, and J.M. Nerbonne. 2008. Distinct cellular and molecular mechanisms underlie functional remodeling of repolarizing K$^+$ currents with left ventricular hypertrophy. *Circ. Res.* 102:1406–1415. https://doi.org/10.1161/CIRCRESAHA.107.170050

Mazuski, C., J.H. Abel, S.P. Chen, T.O. Hermanstyne, J.R. Jones, T. Simon, F.J. Doyle III, and E.D. Herzog. 2018. Entrainment of circadian rhythms depends on firing rates and neuropeptide release of VIP SCN neurons. *Neuron.* 99:555–563.e5. https://doi.org/10.1016/j.neuron.2018.06.029

Meredith, A.L., S.W. Wiler, B.H. Miller, J.S. Takahashi, A.A. Fodor, N.F. Ruby, and R.W. Aldrich. 2006. BK calcium-activated potassium channels regulate circadian behavioral rhythms and pacemaker output. *Nat. Neurosci.* 9:1041–1049. https://doi.org/10.1038/nn1740

Michel, S., and J.H. Meijer. 2020. From clock to functional pacemaker. *Eur. J. Neurosci.* 51:482–493. https://doi.org/10.1111/ejn.14388

Miyake, A., S. Mochizuki, H. Yokoi, M. Kohda, and K. Furuichi. 1999. New ether-à-go-go K$^+$ channel family members localized in human telencephalon. *J. Biol. Chem.* 274:25018–25025. https://doi.org/10.1074/jbc.274.35.25018

Montgomery, J.R., J.P. Whitt, B.N. Wright, M.H. Lai, and A.L. Meredith. 2013. Mis-expression of the BK K$^+$ channel disrupts suprachiasmatic nucleus circuit rhythmicity and alters clock-controlled behavior. *Am. J. Physiol. Cell Physiol.* 304:C299–C311. https://doi.org/10.1152/ajpcell.00302.2012

Nunez, A.A., A. Bult, T.L. McElhinny, and L. Smale. 1999. Daily rhythms of Fos expression in hypothalamic targets of the suprachiasmatic nucleus in diurnal and nocturnal rodents. *J. Biol. Rhythms.* 14:300–306. https://doi.org/10.1177/074873099129000713

Panda, S., M.P. Antoch, B.H. Miller, A.I. Su, A.B. Schook, M. Straume, P.G. Schultz, S.A. Kay, J.S. Takahashi, and J.B. Hogenesch. 2002. Coordinated

Hermanstyne et al.
Kv12 channels regulate nighttime SCN neuronal firing

Journal of General Physiology   22 of 23
https://doi.org/10.1085/jgp.202213310

transcription of key pathways in the mouse by the circadian clock. *Cell.* 109:307–320. https://doi.org/10.1016/S0092-8674(02)00722-5

Patton, A.P., M.D. Edwards, N.J. Smyllie, R. Hamnett, J.E. Chesham, M. Brancaccio, E.S. Maywood, and M.H. Hastings. 2020. The VIP-VPAC2 neuropeptidergic axis is a cellular pacemaking hub of the suprachiasmatic nucleus circadian circuit. *Nat. Commun.* 11:3394. https://doi.org/10.1038/s41467-020-17110-x

Paul, J.R., D. DeWoskin, L.J. McMeekin, R.M. Cowell, D.B. Forger, and K.L. Gamble. 2016. Regulation of persistent sodium currents by glycogen synthase kinase 3 encodes daily rhythms of neuronal excitability. *Nat. Commun.* 7:13470. https://doi.org/10.1038/ncomms13470

Paul, J.R., R.L. Johnson, R.S. Jope, and K.L. Gamble. 2012. Disruption of circadian rhythmicity and suprachiasmatic action potential frequency in a mouse model with constitutive activation of glycogen synthase kinase 3. *Neuroscience.* 226:1–9. https://doi.org/10.1016/j.neuroscience.2012.08.047

Pennartz, C.M., M.T. De Jeu, A.M. Geurtsen, A.A. Sluiter, and M.L. Hermes. 1998. Electrophysiological and morphological heterogeneity of neurons in slices of rat suprachiasmatic nucleus. *J. Physiol.* 506:775–793. https://doi.org/10.1111/j.1469-7793.1998.775bv.x

Reppert, S.M., and D.R. Weaver. 2001. Molecular analysis of mammalian circadian rhythms. *Annu. Rev. Physiol.* 63:647–676. https://doi.org/10.1146/annurev.physiol.63.1.647

Schmittgen, T.D., and K.J. Livak. 2008. Analyzing real-time PCR data by the comparative C_T method. *Nat. Protoc.* 3:1101–1108. https://doi.org/10.1038/nprot.2008.73

Schwartz, W.J., R.A. Gross, and M.T. Morton. 1987. The suprachiasmatic nuclei contain a tetrodotoxin-resistant circadian pacemaker. *Proc. Natl. Acad. Sci. USA.* 84:1694–1698. https://doi.org/10.1073/pnas.84.6.1694

Sokolove, P.G., and W.N. Bushell. 1978. The chi square periodogram: Its utility for analysis of circadian rhythms. *J. Theor. Biol.* 72:131–160. https://doi.org/10.1016/0022-5193(78)90022-X

Stegmeier, F., G. Hu, R.J. Rickles, G.J. Hannon, and S.J. Elledge. 2005. A lentiviral microRNA-based system for single-copy polymerase II-regulated RNA interference in mammalian cells. *Proc. Natl. Acad. Sci. USA.* 102:13212–13217. https://doi.org/10.1073/pnas.0506306102

Trudeau, M.C., S.A. Titus, J.L. Branchaw, B. Ganetzky, and G.A. Robertson. 1999. Functional analysis of a mouse brain Elk-type K^+ channel. *J. Neurosci.* 19:2906–2918. https://doi.org/10.1523/JNEUROSCI.19-08-02906.1999

Whitt, J.P., J.R. Montgomery, and A.L. Meredith. 2016. BK channel inactivation gates daytime excitability in the circadian clock. *Nat. Commun.* 7: 10837. https://doi.org/10.1038/ncomms10837

Zagotta, W.N., T. Hoshi, and R.W. Aldrich. 1990. Restoration of inactivation in mutants of Shaker potassium channels by a peptide derived from ShB. *Science.* 250:568–571. https://doi.org/10.1126/science.2122520

Zhang, X., F. Bertaso, J.W. Yoo, K. Baumgärtel, S.M. Clancy, V. Lee, C. Cienfuegos, C. Wilmot, J. Avis, T. Hunyh, et al. 2010. Deletion of the potassium channel Kv12.2 causes hippocampal hyperexcitability and epilepsy. *Nat. Neurosci.* 13:1056–1058. https://doi.org/10.1038/nn.2610

Zhang, X., B. Bursulaya, C.C. Lee, B. Chen, K. Pivaroff, and T. Jegla. 2009. Divalent cations slow activation of EAG family K^+ channels through direct binding to S4. *Biophys. J.* 97:110–120. https://doi.org/10.1016/j.bpj.2009.04.032

Zou, A., Z. Lin, M. Humble, C.D. Creech, P.K. Wagoner, D. Krafte, T.J. Jegla, and A.D. Wickenden. 2003. Distribution and functional properties of human KCNH8 (Elk1) potassium channels. *Am. J. Physiol. Cell Physiol.* 285:C1356–C1366. https://doi.org/10.1152/ajpcell.00179.2003
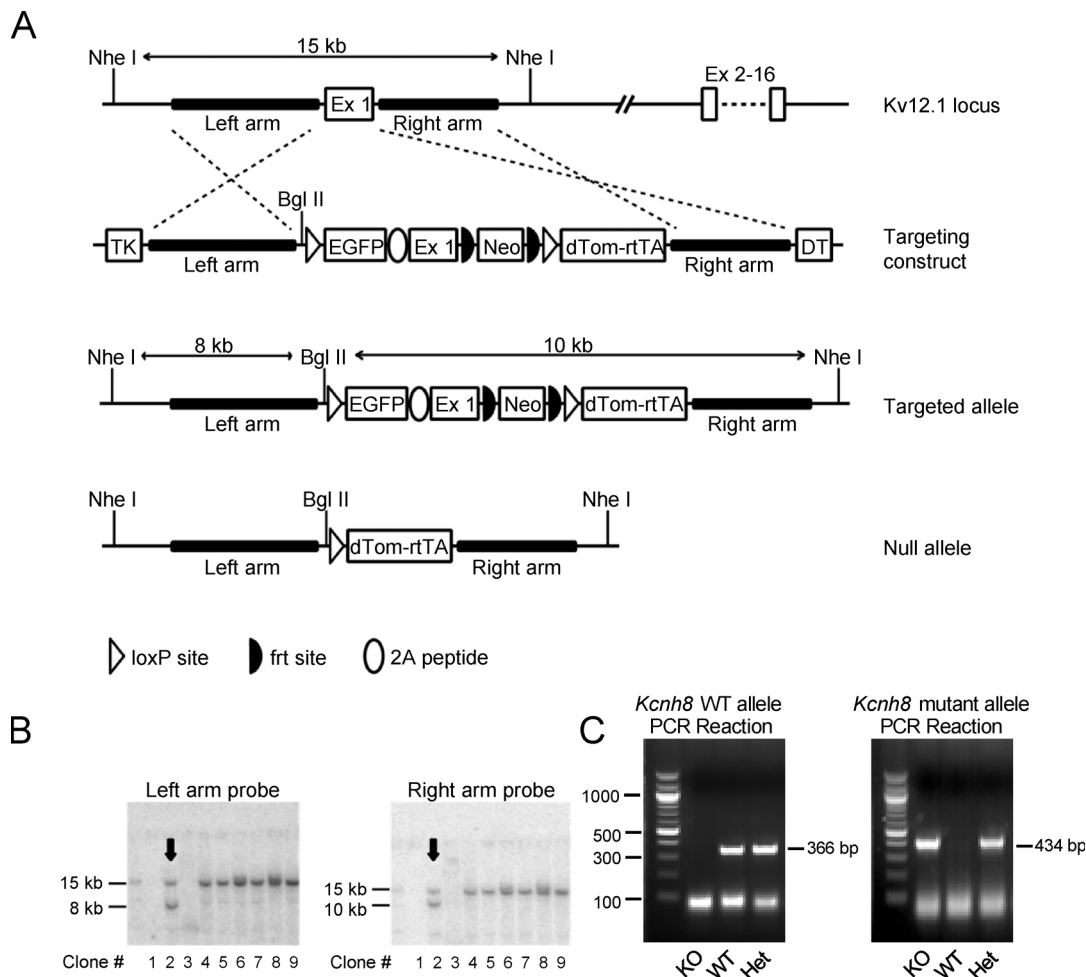
Supplemental material

Figure S1. Generation of (Kv12.1$^{-/-}$) mice harboring a targeted disruption of the *Kcnh3* locus. (A) Schematic of the targeted exon 1 *Kcnh8* (Ex1) locus, the linearized targeting construct, the initial targeted allele, and the null (knockout) allele generated by Cre-loxP recombination. Targeting of the mouse *Kcnh8* (Kv12.1) locus involved homologous recombination (dashed lines) in mouse embryonic stem cells between the native *Kcnh8* locus and the targeting vector, and insertion of a loxP site and myristoyl-EGFP into Ex1 immediately upstream of the translation start. A viral 2A sequence joins the myristoyl-EGFP open reading frame to the Kv12.1 open reading frame to potentially allow EGFP-labeling of Kv12.1-expressing cells carrying the targeted allele. Downstream of Ex1 in the first intron, insertions include an frt-bracketed neomycin resistance cassette (Neo) driven by the PGK promoter for positive selection of targeted ES cells on G418, a second loxP site, and dTomato-2A-rtTA (reverse tetracycline trans-activator) cassette (dTOM-rtTA) which includes an SV40 polyadenylation sequence to terminate transcription and block expression of downstream exons. TK (thymidine kinase) and DT (diptheria toxin) expression cassettes flank the left and right, respectively, arms in the targeting construct. These negative selection cassettes are eliminated by homologous recombination but were included to suppress the random insertion of the targeting construct into the ES cell genome. Note the native allele is bracketed by Nhe I restriction sites ~15 Kb apart. In the targeted allele, the Nhe I sites are preserved, but the distance between them is increased to ~18 Kb, and a unique Bgl II site is introduced upstream of the 5′ loxP site. Hybridization probes located between either (left or right) arm and the neighboring Nhe I site will label a ~15 Kb band in a Southern blot of Nhe I/Bgl II digested genomic DNA for the WT allele. The same probes will label bands of 8 Kb (left arm) and 10 Kb (right arm) for the targeted allele. **(B)** Southern blot analysis of nine G418-resistant ES cell clones following Nhe I/Bgl II digestion of genomic DNA with a probe upstream of the left arm (left) or downstream of the right arm (right). The WT allele is identified by the 15-kb band with both probes, whereas the targeted allele is identified by 8-kb (left arm) and 10-kb (right arm) bands. Arrows indicate the ES cell clone as positive for carrying the targeted allele used to generate the Kv12.1$^{-/-}$ mouse line. Note that DNA isolation failed for two clones (clones #1 and 3). The complete gels from which the "cut outs" in B were derived are provided in the source data. **(C)** ES clone #2 was karyotyped to confirm chromosome number and morphology and used for injection into C57BL/6J blastocysts. Three male chimeric mice were obtained, two of which transmitted the targeted allele through the germline. Mice carrying the targeted allele were bred with C57BL/6J-TgN(Zp3-Cre)93Knw females, which express Cre-recombinase in the germline (Kemler et al., 2004), to generate heterozygous Kv12.1$^{+/-}$ animals, which were then bred to generate Kv12.1$^{-/-}$ mice. For genotyping, a two-step PCR reaction was used with primers specific to the WT (sense: 5′-TGGTCACAGTGCAGCGGCCAGGGAGTA-3′ and antisense: 5′-AAATTA TTGCGCGGATGGAAACAGAGGA-3′) and targeted (sense: 5′-GTCACAGTGCAGCGGCCAGGGAGTAGC-3′ and antisense: 5′-CTTGGCGGTCTGGGTGCCCTCGTAGG-3′) alleles for the *Kcnh8* gene. Bands at both 366 (WT) and 434 bp (targeted) identified heterozygous Kv12.1$^{+/-}$ mice; bands at only 366 or 434 bp identified WT or homozygous Kv12.1$^{-/-}$ mice, respectively. Source data are available for this figure: SourceData FS1.
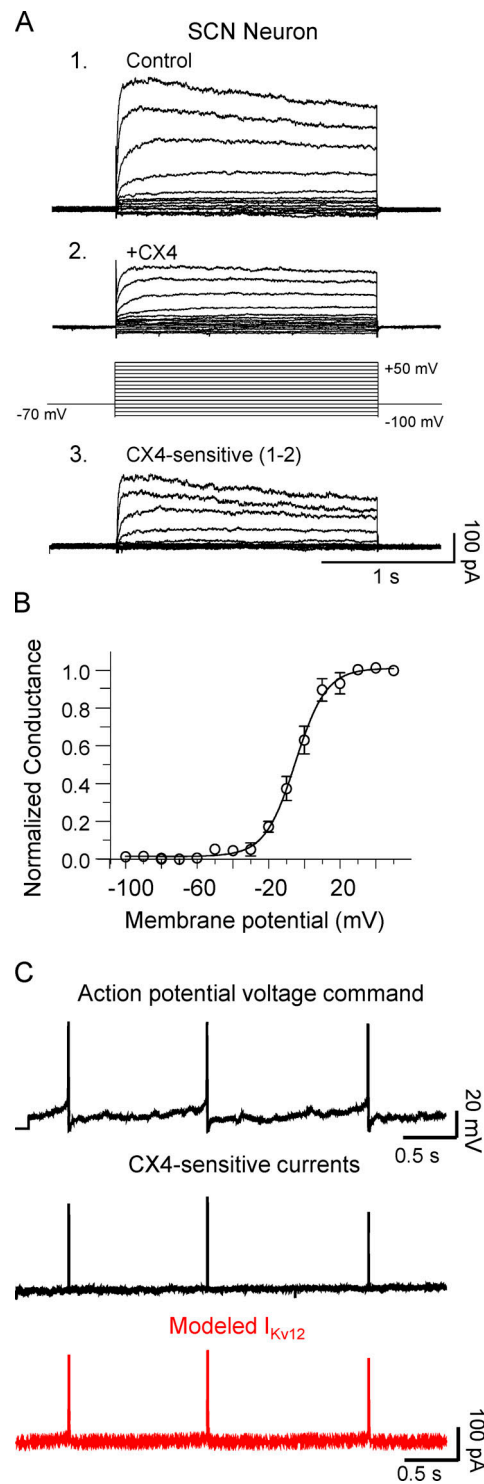
Figure S2. **CX4-sensitive currents in WT SCN neurons and Cybercyte modeled I_{Kv12}. (A)** Representative whole-cell Kv current recordings obtained from an SCN neuron in an acute slice prepared from a night-phased (ZT19–ZT24) WT SCN are shown. Whole-cell Kv currents, evoked during (2 s) voltage steps to potentials ranging from −100 to +50 mV (in 10 mV increments) from a holding potential of −70 mV, were first recorded in ACSF bath solution with 10 mM TEA and 10 mM 4-AP added (A1) and again following superfusion of the 10 mM TEA- and 10 mM 4-AP-containing ACSF with 20 µM CX4 added (A2). The voltage-clamp paradigm (in gray) is illustrated below the current records. Offline digital subtraction of the records obtained in the presence (A2), from the currents recorded in the absence (A1), of 20 µM CX4 provided the CX4-sensitive currents (A3). I_{CX4} conductances at each test potential were calculated and normalized to the maximal conductance (G_{max}), determined in the same cell. **(B)** The mean ± SEM normalized conductances of activation of the CX4-sensitive currents are plotted as a function of the test potential and fitted with single Boltzmanns. The $V_{1/2}$ and the k values derived from these fits for current activation were $V_{1/2}$ = −4.9 ± 1.0 mV; k = 8.7 ± 1.9 (n = 21). **(C)** These parameters were used to tune the I_{K12} model to fit the CX4-sensitive currents that were recorded during action potential–clamp experiments (see Fig. 4). The properties of currents produced by the Cybercyte I_{Kv12} model (lower panel, red) reliably reproduce the CX4-sensitive currents measured in action potential–clamp recordings (middle panel, black) from WT SCN neurons.
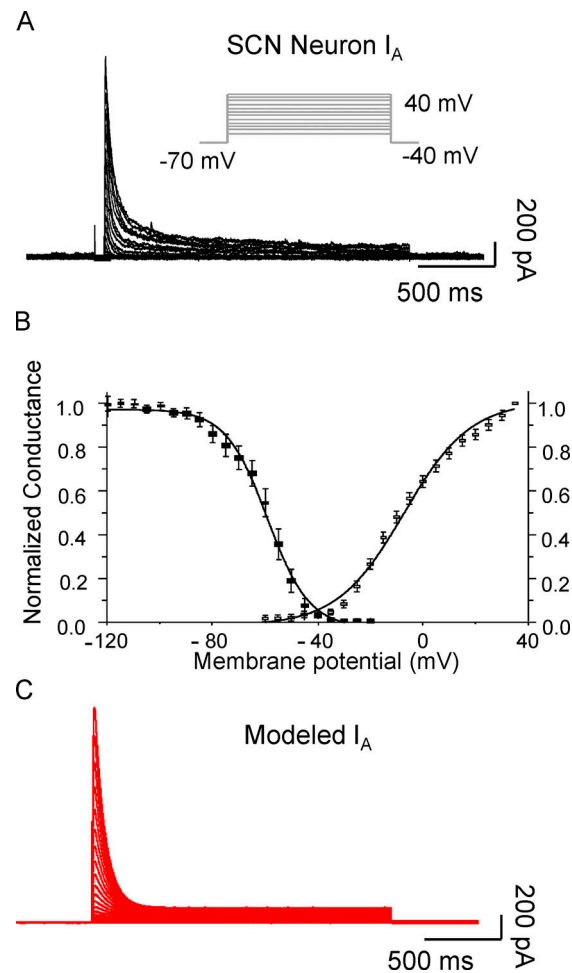
Figure S3. **Cybercyte modeled I$_A$.** A Markov model describing the gating of the K$^+$ channels that generate I$_A$ in WT SCN neurons was developed based on a previously described model of the rapidly activating and inactivating, I$_A$-like, K$^+$ current in (ferret) ventricular myocytes (Campbell et al., 1993), and was populated using previously acquired voltage-clamp data detailing the time- and voltage-dependent properties of I$_A$ in mouse SCN neurons (Hermanstyne et al., 2017). **(A)** Representative I$_A$ waveforms recorded from a WT SCN neuron (Hermanstyne et al., 2017) in response to voltage steps to test potentials ranging from −40 to +40 mV (in 5 mV increments) from a HP of −70 mV are shown; the voltage-clamp paradigm is illustrated above the current records. **(B)** The voltage-dependences of activation and inactivation for I$_A$ in WT SCN neurons (Hermanstyne et al., 2017) were determined using protocols identical to those described above for the CX4-senstive currents. The V$_{1/2}$ and the k values derived from these fits for current activation (open symbols) and inactivation (closed symbols) were V$_{1/2}$ = −9.3 ± 1.3 mV; k = 12.7 ± 0.8 (n = 12) and V$_{1/2}$ = −59.4 ± 2.1 mV, k = 7.9 ± 0.7 (n = 12), respectively. **(C)** These parameters were used to tune the model. **(C)** The waveforms of the currents produced by the Cybercyte I$_A$ model reliably reproduced I$_A$ recorded from WT SCN neurons (A).
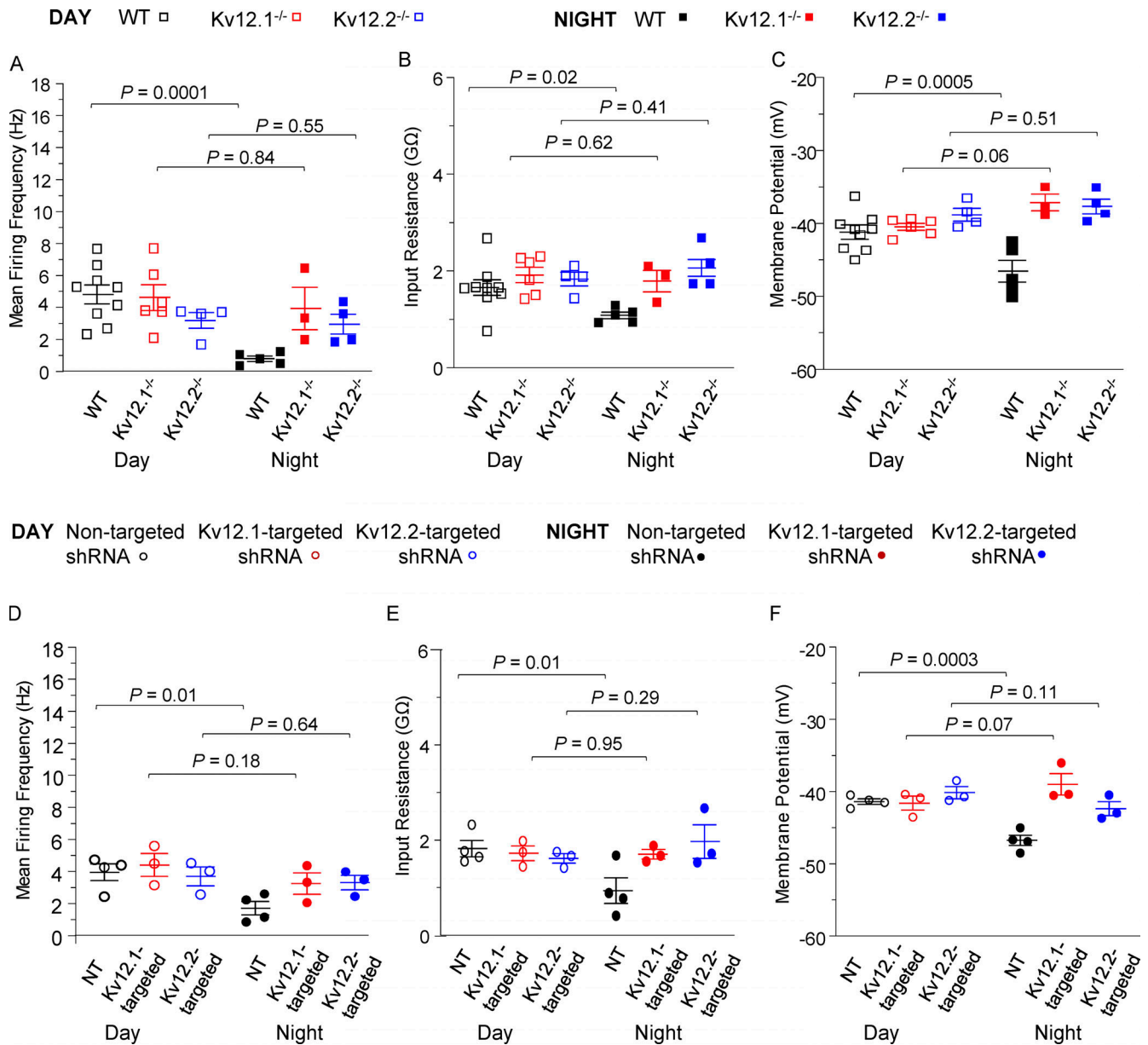
Figure S4. **Repetitive firing rates in individual Kv12.1$^{-/-}$, Kv12.2$^{-/-}$, Kv12.1-targeted shRNA-expressing, and Kv12.2-targeted shRNA-expressing animals/slices.** Comparisons of repetitive firing rates and membrane properties of WT (black squares), Kv12.1$^{-/-}$ (red squares), Kv12.2$^{-/-}$ (blue squares), NT shRNA-expressing (black circles), Kv12.1-targeted shRNA-expressing (red circles), and Kv12.2-targeted shRNA-expressing (blue circles) daytime (ZT 7–ZT 12; open symbols) and nighttime (ZT 18–ZT 24; closed symbols) SCN neurons; the individual data points represent the average values determined in slices from individual animals; N = number of animals. **(A–C)** Repetitive firing rates (A), input resistances (B), and membrane potentials (C) were measured in WT, Kv12.1$^{-/-}$, and Kv12.2$^{-/-}$ SCN neurons in slices prepared during the day (open symbols: N = 9 for WT [black square]; N = 6 for Kv12.1$^{-/-}$ [red square]; N = 4 for Kv12.2$^{-/-}$ [blue square]) or at night (closed symbols: N = 5 for WT [black square]; N = 3 for Kv12.1$^{-/-}$ [red square]; N = 4 for Kv12.2$^{-/-}$ [blue square]) and average values (in individual slices/animals) are plotted. **(D–F)** Average daytime and nighttime repetitive firing rates (D), input resistances (E), and membrane potentials (F), determined in daytime (open symbols) NT shRNA- (black circles; N = 4), Kv12.1-targeted shRNA- (red circles; N = 3), Kv12.2-targeted shRNA- (blue circles; N = 3), and nighttime (closed symbols) NT shRNA- (black circles; N = 4), Kv12.1-targeted shRNA- (red circles; N = 3), and Kv12.2-targeted shRNA- (blue circles; N = 3) expressing SCN neurons are presented. In A–F, mean ± SEM values are plotted and P values are indicated. All data are also tabulated in Table S1.
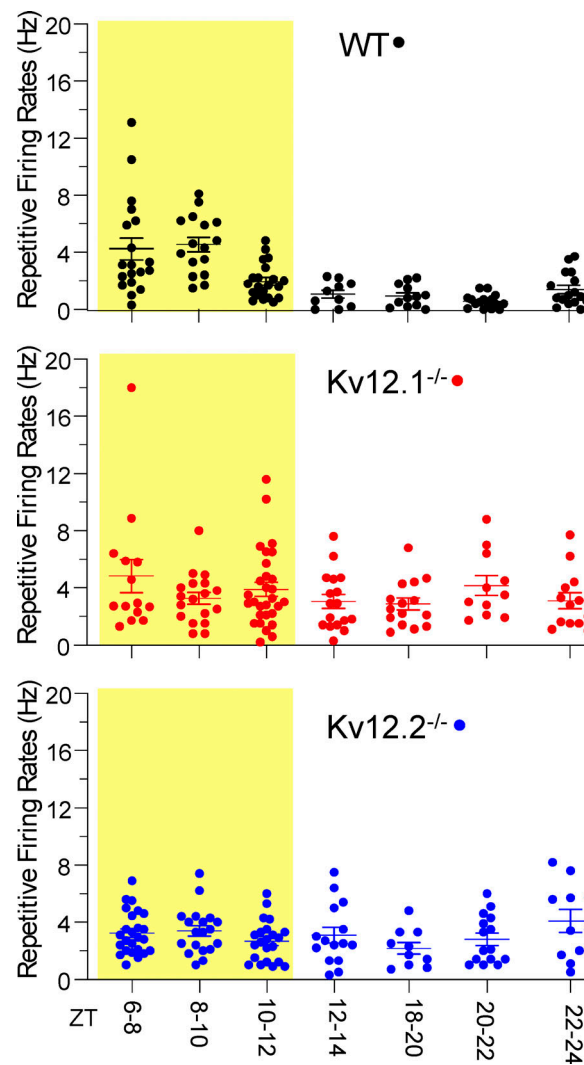
Hermanstyne et al.
Kv12 channels regulate nighttime SCN neuronal firing

Journal of General Physiology   S5
https://doi.org/10.1085/jgp.202213310

Figure S5. Repetitive firing rates of Kv12.1$^{-/-}$ and Kv12.2$^{-/-}$ SCN neurons are higher than in WT SCN neurons throughout the night. Cell-attached voltage recordings were obtained for WT, Kv12.1$^{-/-}$, and Kv12.2$^{-/-}$ SCN neurons in acute slices prepared at various times throughout the circadian cycle. As is evident, mean ± SEM peak firing rates were high throughout the day (yellow shaded region) in WT (black circles) SCN neurons (n = 132), subsequently decreased during the transition from day to night, and remained low throughout the night. Conversely, the mean ± SEM peak firing rates of Kv12.1$^{-/-}$ (red circles; n = 121) and Kv12.2$^{-/-}$ (blue circles; n = 125) SCN neurons did not vary measurably over time and were consistently high (similar to the daytime repetitive firing rates of WT SCN neurons) throughout the day and night.
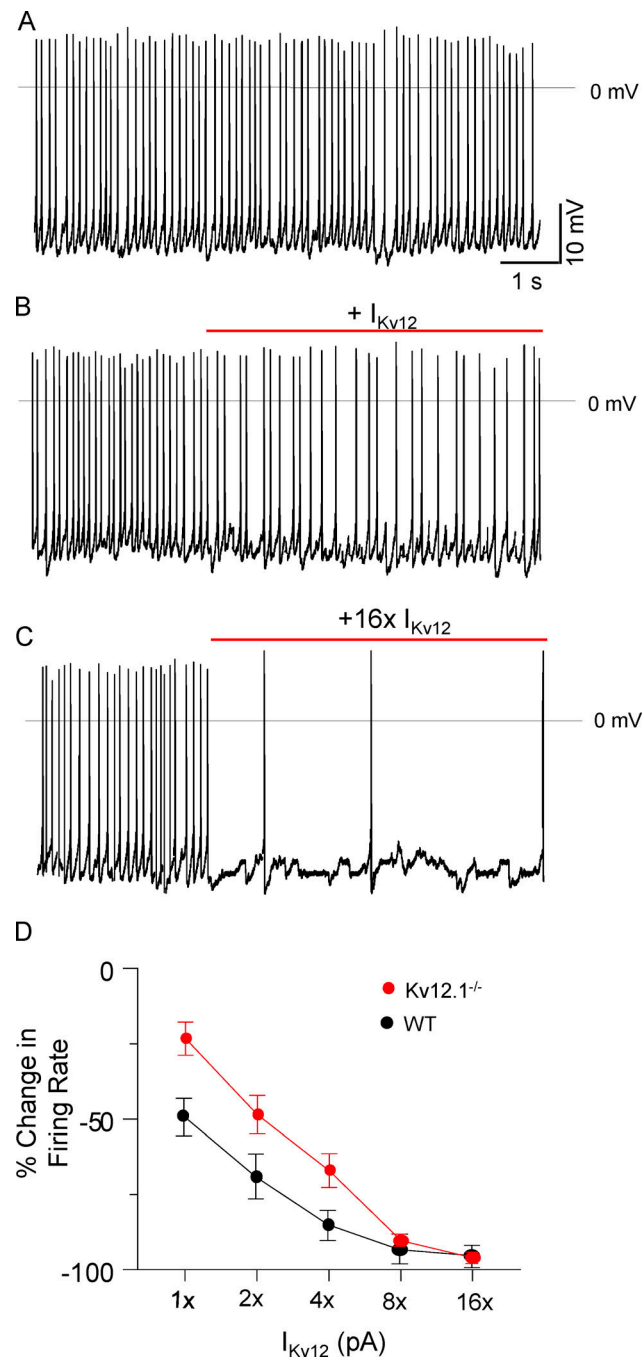
Figure S6. Dynamic clamp-mediated addition of I_{Kv12} decreases the rate of repetitive firing in nighttime Kv12.1$^{-/-}$ SCN neurons. (A–C) Representative whole-cell current-clamp recordings obtained from a nighttime (ZT18–ZT20) Kv12.1$^{-/-}$ SCN neuron under control conditions (A) and with dynamic clamp-mediated addition of modeled I_{Kv12} (B and C). Similar to WT SCN neurons (see Fig. 7), the addition of modeled I_{Kv12} (B and C) reduced the repetitive firing rates of Kv12.1$^{-/-}$ SCN neurons in direct proportion to the amplitude of the injected current. **(D)** The mean ± SEM (n = 11) percentage changes in the repetitive firing rates of nighttime Kv12.1$^{-/-}$ SCN neurons (red circles) are plotted as a function of the amplitude of I_{Kv12} added. The percent changes in the repetitive firing rates of WT neurons with the addition of I_{Kv12} (from Fig. 7 D) are replotted here (black circles) to facilitate direct comparison of the results in WT and Kv12.1$^{-/-}$ SCN neurons.
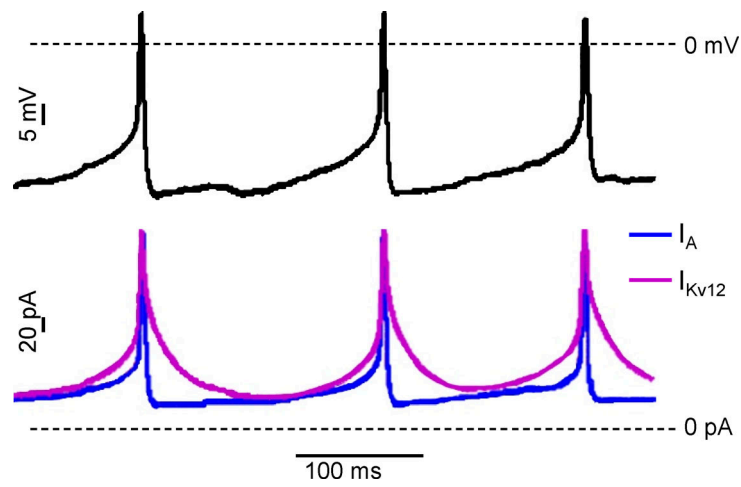
Figure S7.   **Kinetic differences between the Cybercyte modeled I$_A$ and I$_{Kv12}$.** Comparison of the normalized currents produced by the Cybercyte I$_{Kv12}$ (lower panel, purple) and I$_A$ (lower panel, blue) models generated by action potential waveforms (upper panel, black) from a representative WT SCN neuron.
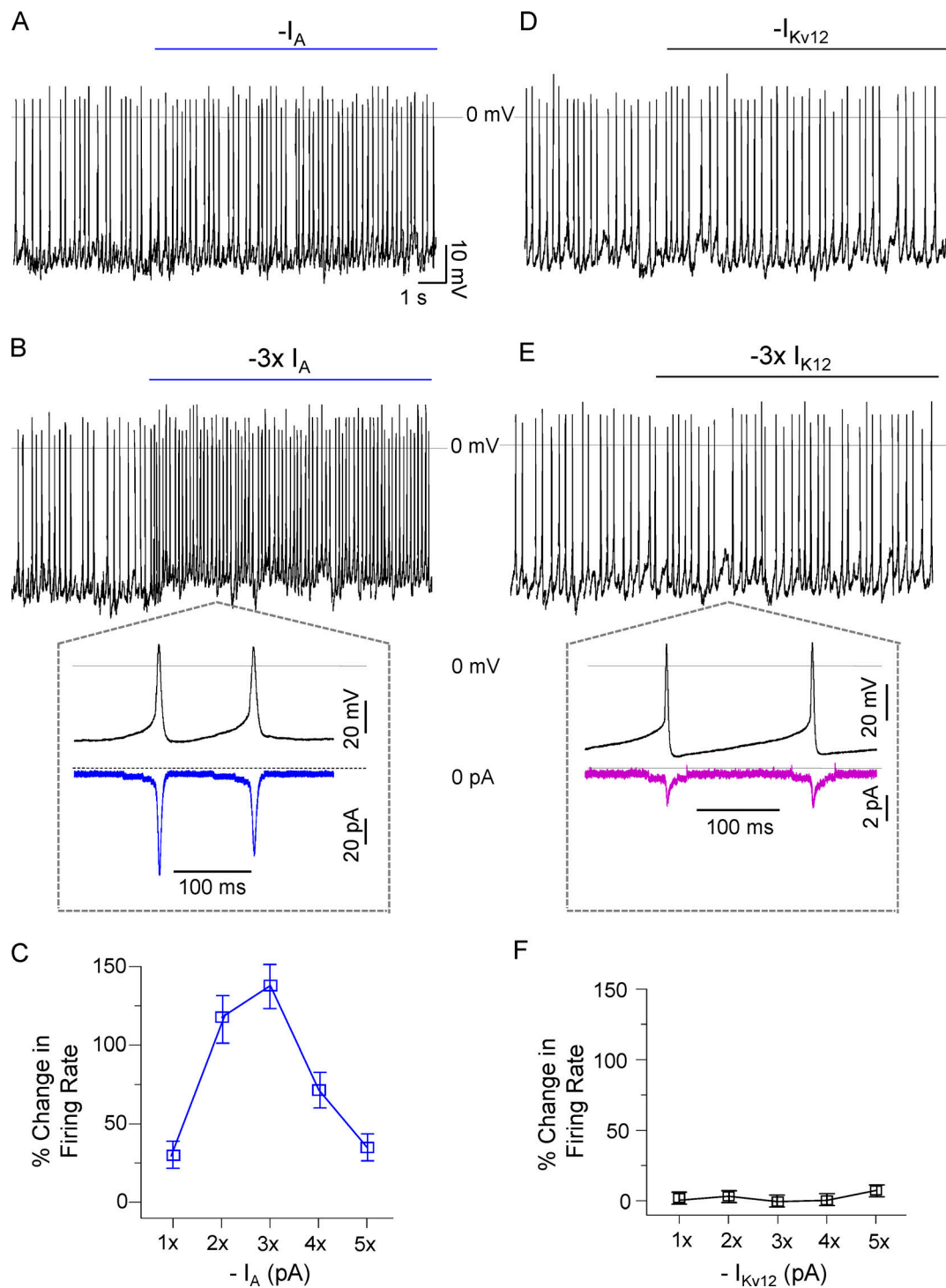
Figure S8. **Direct comparison of the effects of dynamic clamp-mediated subtraction of I_{Kv12} versus I_A in daytime WT SCN neurons. (A, B, D, and E)** Representative whole-cell current-clamp recordings were obtained from a day-phased (ZT7–ZT12) WT SCN neuron with dynamic clamp-mediated subtraction of modeled I_A (A and B) or I_{Kv12} (D and E). Subtracting modeled 1x or 3x I_A increased the rate of repetitive firing (A and B), whereas subtracting modeled 1x or 3x I_{Kv12} (D and E) in the same cell did not measurably alter the firing rate. In the insets below B and E, the waveforms of individual action potentials (black), recorded in a representative WT daytime SCN neuron with subtracted modeled (−3x) I_A (B) or (−3x) I_{Kv12} (E), are plotted on an expanded timescale. The modeled (−3x) I_A (blue, B) and (−3x) I_{Kv12} (purple, E) waveforms in these cells are shown; the zero current levels are indicated by the dotted lines. Similar results were obtained in six additional cells. **(C and F)** Plotting the mean ± SEM ($n = 7$) percentage changes in the repetitive firing rates of daytime WT SCN neurons reveals the mark difference in the effects of subtracting I_A (C) versus I_{Kv12} (F).
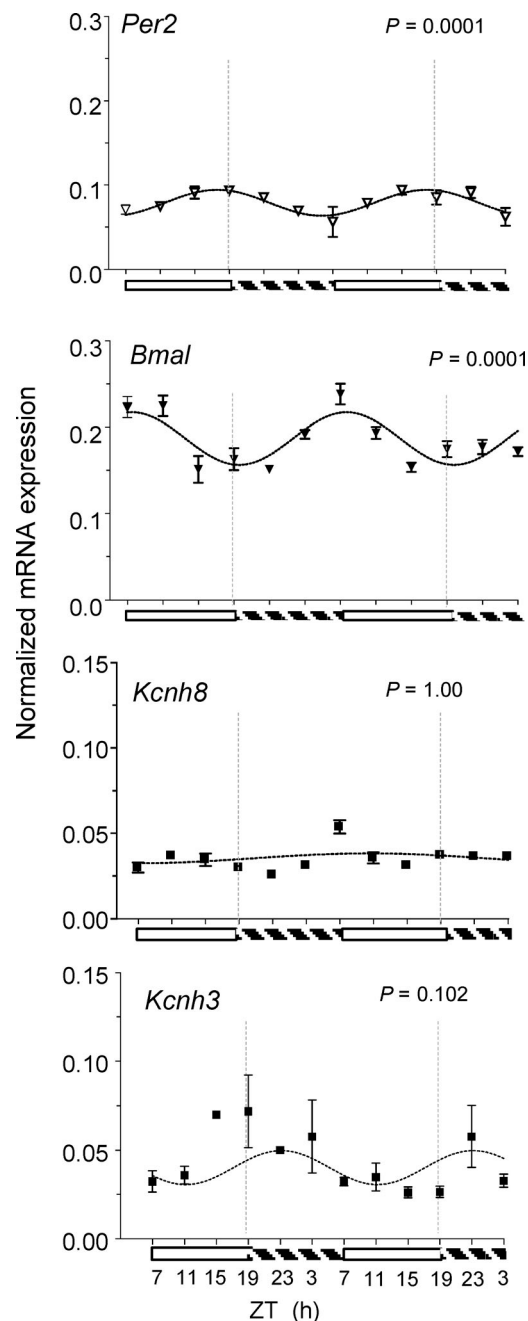
Figure S9. **Expression of *Kcnh8* and *Kcnh3* in the SCN.** The expression levels of the transcripts encoding *Per2*, *Bmal*, *Kcnh8*, and *Kcnh3* were determined by quantitative RT-PCR analyses of SCN tissues samples, obtained every 4 h over a 48 h time-period, from animals maintained in the standard and reversed 12: 12 h LD conditions, as described in Materials and methods. The expression of each transcript was normalized to the expression of *Hprt* in the same sample. Mean ± SEM (*n* = 7–8) values for each transcript are plotted. Fitting the mean data for each transcript, using JTK cycle analysis (Hughes et al., 2010) with the period set to 24 h, reveals that, as expected (Kuhlman and McMahon, 2006; Hastings et al., 2019), the *Per2* (P = 0.0001) and *Bmal* (P = 0.0001) transcripts display 24 rhythms in expression. In contrast, the expression levels of the *Kcnh8* (P = 1.00) and *Kcnh3* (P = 0.102) transcripts do not display 24 h rhythms. The dashed lines on days 1 and 2 are at 7 pm.

Provided online is Table S1. Table 1 shows average active and resting membrane properties of WT, Kv12.1$^{−/−}$, Kv12.2$^{−/−}$, NT, Kv12.1-targeted, and Kv12.2-targeted shRNA-expressing SCN neurons during the day and at night.

Hermanstyne et al.
Kv12 channels regulate nighttime SCN neuronal firing

Journal of General Physiology   S10
https://doi.org/10.1085/jgp.202213310